Preparation of Nitrogen-Doped Carbon Materials for the Reduction of 4-Nitrophenol

Jesse Ponkamo

Acknowledgements

I would like to thank the faculty and staff at the University of Turku Department of Chemistry for fostering a stress-free working and learning environment. As a returning student I am grateful that Professor Kvarnström accepted my application to join the materials chemistry group and to continue my education. In particular the doctoral students were invaluable in preparing this work offering insight and a great deal of expertise on the various tasks set before me. Finally, I would like to thank Dr. Mikko Salomäki for suggesting this research topic and continuing the line of research involving graphene-oxide based materials at the materials chemistry research group.

Table Of Contents

Abbreviations

GO	Graphene Oxide
GRM	Graphene and Related Material
C/O	Carbon to Oxygen Ratio
rGO	Reduced Graphene Oxide
C/N	Carbon to Nitrogen Ratio
CVD	Chemical Vapor Deposition
NMR	Nuclear Magnetic Resonance
FTIR	Fourier Transform Infrared
ATR	Attenuated Total Reflection
DRIFTS	Diffuse Reflectance Infrared Fourier Transform Spectroscopy
UV-Vis	Ultraviolet-Visible
XPS	X-ray Photoelectron Spectroscopy
SEM	Scanning Electron Microscopy
TEM	Transmission Electron Microscopy
AFM	Atomic Force Microscopy
STM	Scanning Tunneling Microscopy
TGA	Thermogravimetric Analysis
ICP-AES	Inductively Coupled Plasma Atomic Emission Spectroscopy
BET	Brunauer Emmet Tiller
XRD	X-ray Diffraction Analysis
4-NP	4-Nitrophenol

H-NG	Hydrothermally Prepared Nitrogen Doped Graphene
F-NG	Furnace Prepared Nitrogen Doped Graphene
HC-BCN Pune	Honeycomb Boron and Nitrogen Doped Carbon from Pune
GCE	Glassy Carbon Electrode
$TBAPF_6$	Tetrabutylammonium Hexafluorophosphate
ACN	Acetonitrile
At. %	Atomic Percent

Abstract

In this work two nitrogen-doped carbon materials were prepared, characterized, and used in modified electrodes for the electrochemical reduction of 4-nitrophenol. The synthesis methods of the two materials were based on two different methods. The first method was pyrolysis of carbon and nitrogen containing source molecules and the second was a hydrothermal synthesis utilizing graphene oxide as starting material and dicyandiamide as nitrogen dopant source. The two materials prepared were characterized by FTIR spectroscopy, Raman spectroscopy, XPS spectroscopy, AFM, SEM. Characterization showed that the materials prepared were nitrogen-doped carbon materials with structure of graphite microplates each showing differing structural and chemical properties from one another. Glassy carbon electrodes coated with the nitrogen-doped carbon materials were prepared and used for the electrochemical reduction of 4-nitrophenol which were analyzed by collecting cyclic voltammograms of the electrochemical process in an electrolyte solution of acetonitrile and tetrabutylammonium hexafluorophosphate. The cyclic voltammograms showed that the nitrogen-doped materials prepared were able to reduce 4-nitrophenol and showed a reduced reduction potential compared to uncoated glassy carbon electrodes. The cyclic voltammograms also broadly demonstrated how the different preparation methods of the nitrogen-doped carbon materials impact structure and their concomitant electrochemical properties.

1. Introduction

The natural world is dependent upon carbon chemistries, which is seen in the elegant biosynthesis of virtually all molecules needed for propagating life on earth. Humans gained a similar power over carbon chemistries with the birth of modern organic chemistry in the 1800s which came into wider industrial utility in the 1900s with the development of the pharmaceutical industry and demand for synthetic polymers. Besides the utility of organic chemistry, coal and charcoal have played roles in the development and propagation of modern society, as medicine and in the smelting forges and boilers that pushed human civilization through the industrial revolution and into the modern era of the petroleum industry. The chemistries of carbon have come into new relief in the last 30 years with the discovery of the carbon allotropes fullerenes, carbon nanotubes, and graphenes. Herein begins an introduction to graphene and related materials regarding chemistry, preparation methods, and characterization which will then conclude with an outline of the original work carried out in this Master's Thesis. The aim of this study being to thread the recent research interest in heteroatom-doped material and electrocatalysts. Following the review and original work section will come the experimental section, detailing the synthetic methods and other protocols used in completing the original work. The penultimate section, results and discussion, will expound upon the characterization of the prepared materials as well as their implementation and results in electrochemistry. A conclusion section will then close this work.

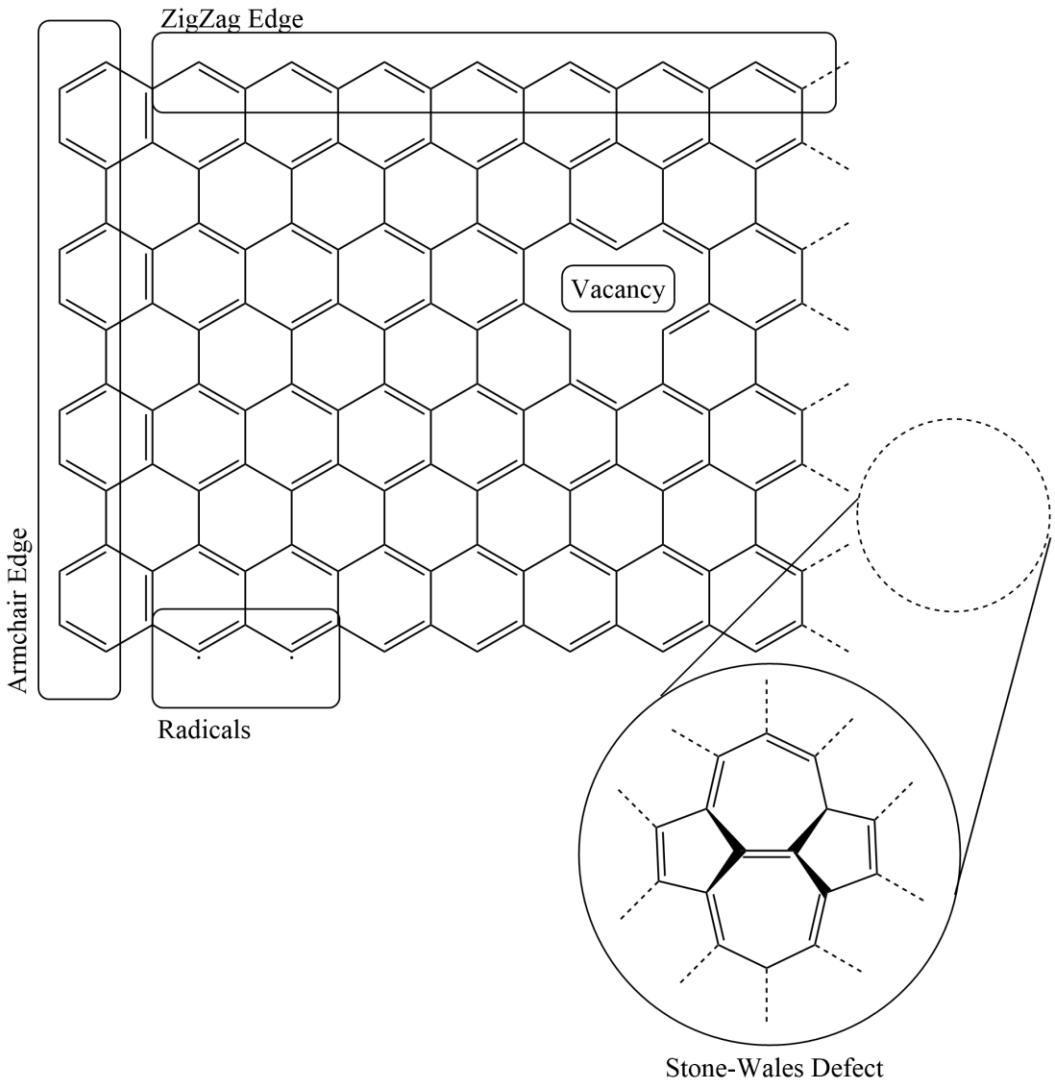

Figure 1. Diagram depicting the structure of graphene highlighting key features and properties inherent in graphene.

Graphene as defined by the most recent IUPAC Gold Book is "a single carbon layer of the graphite structure, describing its nature by analogy to a polycyclic aromatic hydrocarbon of quasi infinite size", (figure 1).[1] Graphene is often referenced as being discovered in 2004 with the paper authored in part by Andre Geim and Konstantin Novoselov, who would later receive the Nobel Prize in physics for their findings. In the landmark paper graphene was isolated by using transparent tape to mechanically exfoliate atomically thin layers of graphene from highly-oriented pyrolytic graphite and their research demonstrated unique electronic properties of graphene.[2] The theoretical concept of graphene, and the name itself, had been in existence since prior to the publication of

the Geim and Novoselov's paper in 2004 going all the way back to 1986 when the term graphene was initially coined arising from the chemistry of graphite intercalation compounds.[3] As is detailed in Geim's reflection on the prehistory of graphene, published in 2012, the earliest known reference to a material related to graphene was in 1859 when British-chemist Benjamin Brodie, exposed graphite to strong acids producing a suspension of crystalline graphite, which Brodie referred to as graphon.[3] This graphon material is now referred to as graphene oxide (GO), a material containing a sheet of polycyclic carbon with oxygen-containing functional groups such as hydroxyl and carbonyl groups bound to the sheet in addition to defects and holes, (figure 2).[4] The term graphene itself was put forth by German-chemist Hanns-Peter Boehm and coworkers in 1986 in a paper on the nomenclature and terminology of graphite intercalation compounds as a proceeding of the International Committee for Characterization and Terminology of Carbon.[3] Since roughly the middle of the last century monolayer graphite and other carbon materials have been studied by chemists and physicists alike, producing a body of science spanning the crystallography of monolayer graphite, Raman spectroscopy of various carbon materials, and different graphite intercalation compounds and their chemistries.[3] This body of knowledge has laid the foundation for the study of these new carbon materials, which encompass not only graphene but other nanostructured carbon allotropes.

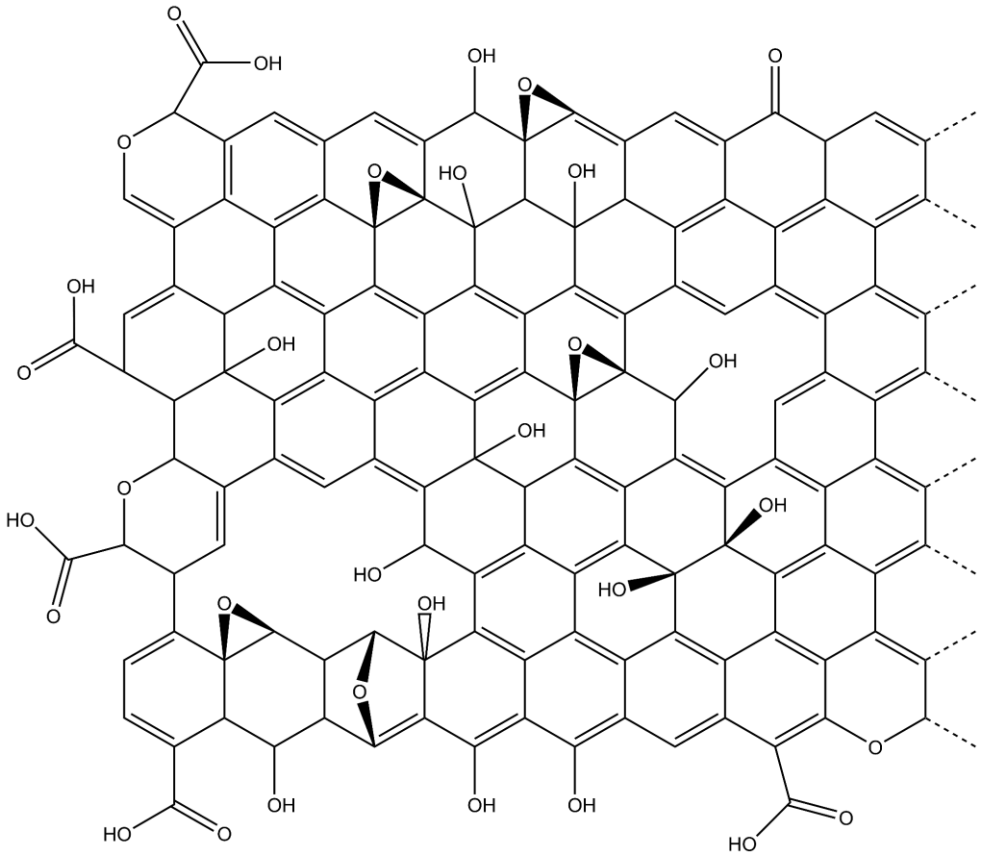

Figure 2. Structure of the Lerf-Klinowski model of graphene oxide.[4]

In the last century carbon allotropes beyond diamond and graphite were eventually discovered to be carbon nanotubes and fullerene.[5,6] Both carbon nanotubes and fullerenes had attracted research interest, and a growing body of scientific literature, prior to 2004.[7] Carbon nanotubes can be described as a sheet of graphene wrapped into a cylinder thus producing a tube of quasi infinite length but a diameter measured in nanometers.[1] Fullerenes on the other hand are discrete molecules typically containing 60 carbon atoms bound together forming a closed sphere which was named in honor of architect and futurist Buckminster Fuller for his famous geodesic domes.[1,5] Looking at the number of publications referencing fullerenes, carbon nanotubes, and graphene in either title or abstract in the last 40 years there is a precipitous increase of interest in the field in the turn of the millennium.[7]

The explosion of interest in graphene has also brought about issues regarding consistency with naming and terminology of the material being prepared and reported upon.[8,9] As can be ascertained

from the IUPAC definition, graphene is a unique and specific material; however, the issue arises from hyphenated materials used in journal article titles and abstracts such as graphene-like, few-layer, and so on. A figure prepared by Wick et al. shows a concise and useful elaboration on a suggested naming scheme based on specific material properties, (figure 3). From a scientific point of view, maintaining brevity in scientific writing regarding these hyphenates, or variations, on the graphene name can create some distance from the graphene definition put forth by IUPAC. The main quality that unites graphene and graphene-like materials is that they are low dimensional, near 2D, carbon nanomaterials, which share unique characteristics and chemistries that diverge from their bulk material. It has been proffered by the European Graphene Flagship to refer to both graphene and graphene-like materials by the title graphene and related material (GRM) when speaking about this broad field of inquiry.[8]

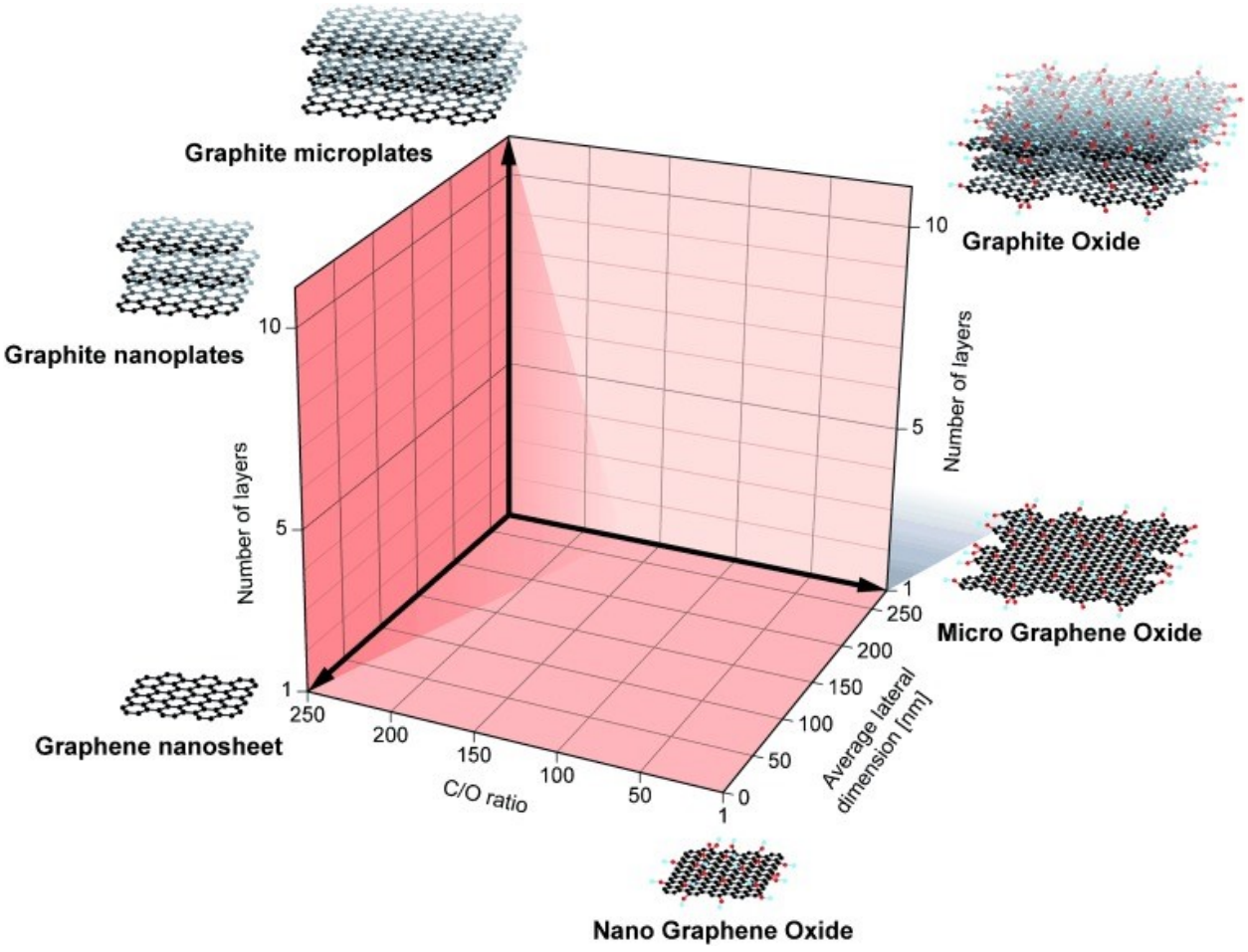

Figure 3. Figures and graph relating dimensionality, layer number, and carbon to oxygen ratio (C/O ratio) to suggested appropriate name. Reproduced with permission from ref. 8 by publisher John Wiley and Sons.

2. Graphene Chemistry

Each carbon atom in the graphene sheet is sp^2 hybridized and bonded to 3 neighboring carbon atoms forming a honeycomb-lattice sheet. This differs from diamond in which the carbon atoms are in tetrahedral configuration with sp^3 hybridization connected solely by σ-bonds and the sheet-like dislocation of bulk graphite is not possible. Graphene and diamond both share a common feature that they are by and large inert, there are reactions which graphene can take part in which will be detailed later. Graphene is fully conjugated with an extended π-system, (figure 1). The extended π-system allows for the delocalization of electrons into the p-orbitals of adjacent carbon atoms, thus producing an electron-rich macromolecule. The delocalization of electrons is what accounts for the conductivity of graphene, as well as in graphite, and it has been shown that electron mobility is exceptionally high in graphene and in fact the behavior of electrons deviates from other semiconductor materials in that they behave as Dirac fermions, or massless particles.[10] A graphene sheet itself is a zero bandgap conductor (semimetal).[2] The bandgap is such that even at room temperature electrons are promoted to the conduction band.[2] A discussion of solid state physics is beyond the realm of this paper; however, the band structure of graphene is exceptional and is what animates a great deal of the solid state physics research and possible application of graphene.

One feature of graphene is the edge structure, it can have what is referred to as zig-zag or armchair structure, (figure 1). It has been shown theoretically and experimentally that size-confined graphene sheets, or nanoribbons, have conductivities that are dependent on their edge structures.[11] Zig-zag being metallic-like while the armchair structure has a bandgap.[11] One such consequence of the zig-zag structure is that it is inherently more reactive than the armchair structure.[12] Radicals that are confined to zig-zag edges, and this edge state is at such a high energy that a planar reconstruction occurs forming the hexagonal, benzenoid structures, into heptagonal or pentagonal

structure to lower the energy of the system.[13] The extended π-system of graphene also enables non-covalent interaction with other aromatic molecules through van der Waals forces.[14]

Theoretically, graphene is a pristine sheet with only the presence of the above-mentioned edge states to provide modulation of the charge distribution of the sheet. In actuality, graphene sheets often contain other edge sites in the form of vacancies and grain boundaries which form naturally or are the result of a preparation method.[12] Grain boundaries and defects also contribute to the modulation of charge on the surface of graphene and in doing so alter the local chemistry, reactivity, and curvature of the graphene sheet.[12] Stone-Wales defect, see figure 1, is a type of defect found in graphene as a result of structural reformation.[15] It has also been shown that regional strain (bending etc.) of the graphene sheet promotes similar changes in charge distribution and the point of the crease is more reactive in certain cases.[16]

Graphene is insoluble and dispersions of graphene tend toward aggregation as the overwhelming van der Waals forces cause re-stacking of the graphene sheets.[17] Covalent functionalization is limited due to the inertness of the basal plane of the graphene sheet leaving only the edges, defect sites, grain boundaries, and points of strain to be functionalized.[18] However, functionalization of graphene is important in not only making modified graphene easily dispersible and stable in organic solvents but in utilizing graphene for different applications.[18]

Many different strategies have been put forth for the functionalization and derivatization of graphene. The most notable derivative is GO. The preparation of GO will be explained in greater detail in section 3.1. Even though GO is a popular material for research there is still some scholarly debate regarding an appropriate model for the general structure and functionality present in GO.[19] However, a commonly referenced model is the Lerf-Klinowski model of GO (figure 2).[4] The Lerf-Klinowski model proposes an ambiguous distribution of epoxy, hydroxyl, ether, and carboxyl groups as well as a mixture of sp^3 and sp^2 hybridized carbons and clustered aromatic or otherwise conjugated carbons.[4] GO is a favorable GRM in that it is hydrophilic, owing to its polar substituents, thus allowing it to be dispersed in a variety of solvents.[20] The different oxygen-containing functional groups, such as epoxides and carbonyls, on GO allow it to be further functionalized by using synthetic methods that take advantage of these oxygen-containing

functional groups. In addition, heteroatom doping is another way to derivatize GRM's to further modify their qualities, in particular modulating the concentration of charge carriers and imbedding functionality into the graphitic network.

As a corollary to the π-conjugation present in graphene cycloaddition reactions, such as Diels-Alder etc., have been shown to take place. Robert Haddon has been active in investigating chemistry of fullerenes and nanotubes and as such has extended this to graphene. An interesting insight Haddon and coworkers discovered is that graphene behaves as both a diene and dienophile in a Diels-Alder reaction and in addition showed that the process is reversible following the retro-Diels-Alder reaction.[21] The diene and dienophile nature of graphene can be rationalized in one manner by the resonance structures which have either diene or dienophile character, (scheme 1).[21] Furthermore, using an analysis of frontier orbital theory and the orbital symmetry present in graphene Haddon and coworkers show that graphene can behave as both a donor and acceptor species.[21] However, as it stands the work of Haddon did not address the fundamental question of whether or not the Diels-Alder reaction was due to the effect of reactive grain boundaries, edges, surface defects, or the effect of underlying substrate. In the case of both Diels-Alder and 1,3-dipolar cycloaddition on pristine graphene it was shown that the basal plane is indeed functionalized by these reactions.[22,23] Mingdi Yan and coworkers showed that aryl nitrene cycloaddition reactions on graphene are affected by the underlying substrate the graphene is deposited on.[24]

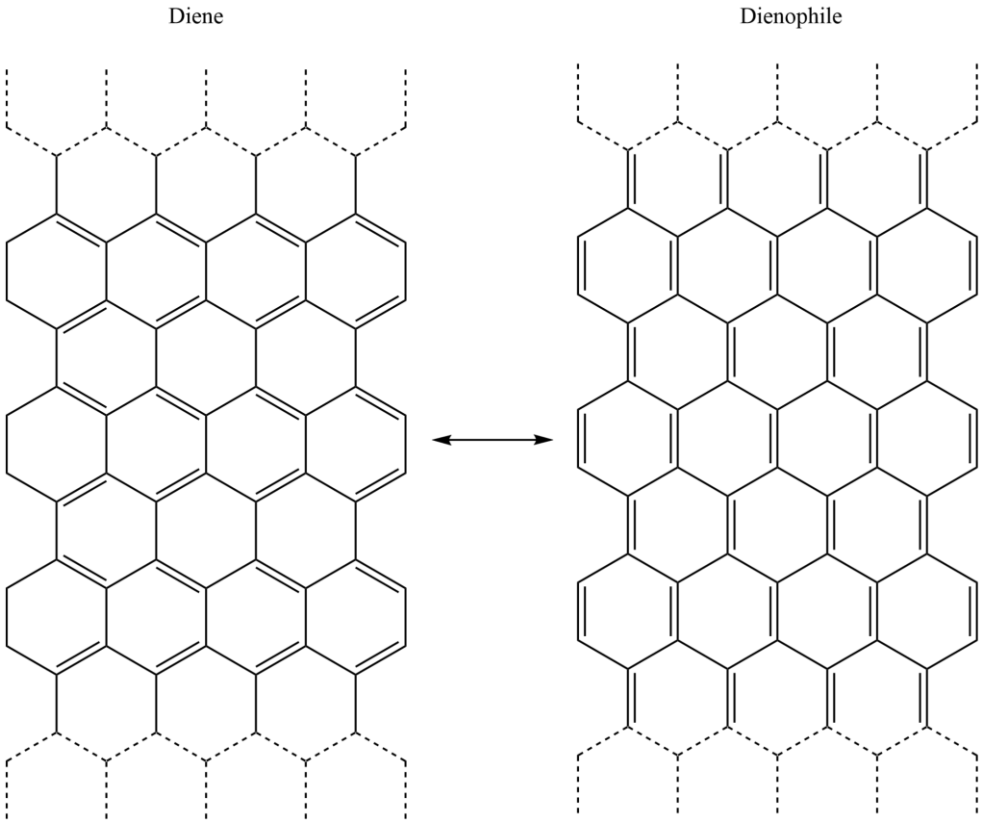

Scheme 1. Resonance structure depicting the diene and dienophile duality of graphene[21].

Beyond cycloaddition reactions the covalent modification of graphene is largely based on chemistries employed in the modification of fullerenes and carbon nanotubes such as those which employ reactive radical species.[25] One often employed method for covalent functionalization of graphene is employing aryl diazonium salts, such a 4-nitrophenyl tetrafluoroborate.[25] Aryl diazonium salts have been employed in functionalizing other carbon materials such as highly oriented pyrolytic graphite, glassy carbon, and carbon nanotubes.[26–28] Typically the reactive aryl radical species are produced from the aryl diazonium salt by means of electrochemical reduction in carbon materials other than graphene; however, graphene's electron rich π-system spontaneously donates an electron thus initiating the radical process.[25,26]

Functionalization of graphene and GRM's ultimately changes the hybridization of the carbon lattice. As more bonds are formed the bonding character is changed from sp^2 to the sp^3 in the newly formed covalent bond, which fundamentally changes the qualities of graphene as the extended π-network becomes fragmented.

3. GRM Preparations Methods

One method for producing graphene has been touched upon, the so-called “scotch tape method”, this is a tedious though simple process, which yields small quantities of graphene and is insufficient for most chemists. This has spurred several approaches to preparing graphene as well as GRM’s. The specific demands of each application or use of GRM’s also dictates the preparation method. Examples of specific needs include pristine and impurity free single-layer graphene for electronic devices. On the other hand catalysts and electrocatalysts benefit from the surface area provided by surface defects and thus fall more under the rubric of GRM’s. In general, preparation methods for GRM’s can be classified into the typical dichotomy of materials synthesis: bottom-up or top-down. Top-down, in which bulk graphite is broken down into individual sheets by mechanical or chemical methods. Bottom-up, in which molecular building blocks are used as precursor materials to form the macromolecule through covalent chemistries. By the time of the writing of this thesis there is what feels like a deluge of different approaches to prepare GRM’s, almost as many for each application, and yet nearly 20 years after the initial paper by Geim and Novoselov there is still ongoing research into the preparation of GRM’s.

3.1 Graphene Oxide

The commonly employed methods for preparing GO today do not differ significantly from the preparation used by Brodie in the 1800’s. The current method is based on a variation of what Hummers et al. proposed in 1958, or as it is cited now as simply the Hummers Method. In the years following 2004 there have been numerous modifications to the Hummers Method, often as a means of producing GO optimized for a specific application or avoiding use of specific reagents or hazardous byproducts. The general concept of all of these different syntheses is that graphite is essentially pried apart into their individual sheets, or exfoliated, by the intercalation of strong acids and oxidizing reagents.[29] The individual oxidizing agents, acids, reaction time, and source carbon affect the overall qualities of the resultant GO.

The Hummers Method entails the following: dispersing powdered flake graphite in concentrated H_2SO_4 to which $NaNO_3$ is added and this mixture is kept at 0°C which is then followed by a careful addition of $KMnO_4$ resulting in exothermic reaction.[30] During this time the graphite is undergoing a process of intercalation in which the acids are being incorporated in between the individual sheets of graphite.[29] With the addition of $KMnO_4$ the intercalated graphite is oxidized increasing the interlayer distance between graphite sheets.[29] Tour and coworkers have shown this process of oxidant intercalation and propagation is diffusion controlled and as such the qualities of the source graphite affect the rate at which the oxidation proceeds such that highly ordered large fragments of graphite take longer than smaller disordered graphite.[29] The resulting mixture is quenched with a portion of water, which is followed by another exothermic reaction, this elevated temperature is maintained at 98°C for 15 minutes.[30] Once the time has elapsed the reaction mixture is allowed to cool for 10 minutes and a mixture of water and H_2O_2 is added to quench the reaction mixture producing another exotherm.[30] With the addition of water the GO sheets delaminate and are thus exfoliated.[29] What follows is a process of purification, filtering, washing to remove as much of the various impurities from the graphite source as well as the permanganate species in solution.[29] Finally, the prepared material can be dried or dispersed into a solvent.

A popular variation on the Hummers Method, the Improved Hummers Method, is largely the same preparation however it calls for the use of H_3PO_4 instead of $NaNO_3$.[31] Avoiding the use of $NaNO_3$ means the synthesis does not produce the hazardous gasses NO_2 and N_2O_4 and this preparation has been shown to be more efficient, producing a higher yield of GO.[31] The improved method also produces a higher oxygen to carbon ratio, however in the resultant chemical reduction the material showed to have excellent qualities for electronics applications.[31] Other variations entail an extra long oxidation reaction time or increasing the amount of $KMnO_4$.[31,32]

3.2 Reduced GO

As has been mentioned GO is a derivative of graphene, lacking in long range order and checkered with oxygen functional groups affecting its performance in applications demanding conductivity as GO is insulating. One strategy utilized to remedy this is to reduce GO, thus reducing a bulk of the oxygen containing and partly restoring the π-network restoring conductivity.[33] Reduced GO (rGO) can be achieved in multiple ways and each method produces a material with different properties such a defect density, surface area, and C/O.

3.2.1 Chemical Reducing Agents

A frequently referenced method used is the chemical reduction using hydrazine hydrate (N_2H_2 in water) which effectively reduces aqueous dispersions of GO.[33] Most reducing agents potent enough to effectively reduce GO are hampered by being incompatible with the typical GO dispersion medium, water. In one study the comparison of C/O of GO starting material to hydrazine hydrate reduced rGO showed a change from 2.7 to 10.3.[33] One observation in regard to the sp^2 carbon network produced from the hydrazine reduction method was that the Raman spectra suggest that the sp^2 domains are smaller in size on average than GO prior to reduction.[33] Hydrazine reduction involves the partial nitrogen-doping of the subsequent rGO leaving a carbon to nitrogen ratio (C/N) of 16.1.[33] One serious concern with scaling up a hydrazine reduction is that hydrazine is a hazardous reducing agent.

One other chemical reductant often featured in the literature is sodium borohydride ($NaBH_4$), a common reducing agent in organic chemistry.[34] A comparison of rGO of a similar C/O prepared with hydrazine and sodium borohydride showed that the latter has a lower sheet resistance.[34] Sodium borohydride reduction also has the added benefit of not leading to nitrogen doping of the resultant rGO.[34] However, it was observed that at a specific lower concentration of sodium borohydride an X-ray photoelectron spectroscopy (XPS) analysis showed the presence of boron oxide complexes while at higher concentrations this was no longer observed.[34]

The growth of green chemistry approaches have also extended to reduction methods of GO. One popular method is the so-called vitamin C (ascorbic acid) reduction.[35,36] Fernández-Merino et al.

found in their comparison of several popular methods for reducing GO, hydrazine hydrate and sodium borohydride among others, showed the ascorbic acid reduction to be effective at producing rGO with a C/O of ~12.5 and conductivity values between 2690 and 7700 S/m.[36] In addition to ascorbic acid, caffeic acid is another green alternative to hydrazine hydrate and sodium borohydride, which produces rGO with a C/O of 7.5.[37]

3.2.2 Hydrothermal and Solvothermal Reduction

Beyond using the above mentioned means of reduction another often cited method is the hydrothermal and solvothermal reduction of GO. Hydrothermal synthesis has been proffered as a green alternative to reduction of GO, all together avoiding the use of classical reducing agents.[38] This method takes advantage of the characteristic chemical properties of a solvent system in a sealed and reinforced vessel at temperature and pressure. Generally, a hydrothermal synthesis is a heterogeneous reaction in an aqueous medium carried out above 100°C and 1 bar.[39] As temperature and pressure increases the dielectric constant, density, and ion product of water changes such that dielectric constant decreases, density decreases, and the ion product of water increases to a maxima at about 250°C and drops precipitously as temperature increases further.[40] At or near supercritical conditions water behaves more like common organic solvents capable of acid/base reactions due to the ion product at these temperatures, which has led to the utilization of hydrothermal conditions for organic chemistry.[41] The source of the reducing power in hydrothermal, and solvothermal conditions using alcohol, is either single electron exchange from hydroxide ions or hydronium ions.[41–43]

K. Loh et al. first reported using hydrothermal synthesis for preparing rGO.[38] The preparation is simple; heating the sealed autoclave with an aqueous dispersion of GO. Based on the reported XPS and solid state ^{13}C NMR spectra of the hydrothermally prepared rGO showed a marked decrease in oxygen functional groups, a C/O of 6.6, and increase in presence of sp^2 carbon suggesting the successful reduction of GO.[38] The greatest drawback to this method in comparison to the chemical reducing agents is the time required and resulting C/O, which both takes longer and does not produce an equally reduced GO. A reduction using 21 mM hydrazine hydrate can be accomplished

in 15 minute reaction time to achieve a C/O of ~12.5 while the hydrothermal method requires up to 10 hours at 200°C to achieve a C/O of ~5.8.[36,44]

Solvents other than water, in so-called solvothermal synthesis, have also been explored in a similar vein to reduce GO. Jaehoon Kim's group did a thorough study of reducing GO in several organic solvents at supercritical conditions which included methanol, ethanol, propanol, butanol, and isopropyl alcohol.[43] The resulting rGO reduced using methanol, ethanol, propanol, butanol, and isopropyl under solvothermal conditions for 2 hours at 400°C had C/O ranging from 10.4, 14.4, 13.7, 12.5, and 13.2, respectively.[43] In analyzing the surface area of the rGO prepared using different alcohols ethanol produced rGO with much higher surface area than the others.[43] The greater surface area is attributed to a more thorough exfoliation of the resulting rGO by ethanol. The C/O of ethanol solvothermal rGO is quite high compared to other methods listed above and the reaction time is also manageable with a 2 hour reaction time, though it does demand the use of a special pressure vessel.

3.2.3 Thermal Reduction

By far the most straightforward and least demanding of technical equipment is the method of reducing GO by thermal reduction in which the sample of GO is placed in a tube furnace, or equivalent, and heated to in excess of 200°C. At temperatures near 100°C adsorbed water is removed and as temperature rises near 200°C oxygen functional groups begin to dissociate and as temperatures continue to rise above 300°C significant mass loss is observed as CO_2 is released and the GO structure begins to lose its carbon network and producing defects in the basal plane of the rGO.[45,46] In Acik et al.'s sprawling analysis of the thermal reduction mechanism of GO they posit that hydroxyl radicals play a key role in initiating the reduction mechanism.[45] At temperatures of 1000°C sp^3 carbon is converted to sp^2 carbon.[46] The C/O content at 127, 300, 400, 500, and 600°C is 5.3, 5.3, 5.8, 10.7, respectively.[46] The remaining oxygen functional groups on rGO at temperatures in excess of 650°C are retained as ethers or carbonyl groups, carbonyls more specifically in the case of multilayer GO due the presence of trapped water in the layers which mediate carbonyl formation.[45] As much as 30-40% of the mass of GO can be lost during the

thermal reduction process in the form of CO and CO_2.[45,46] In Eigler and coworkers thorough analysis of different reduction methods by utilizing statistical Raman analysis showed that thermal reduction of GO at 200°C produced an rGO which was dominated by defects to a much greater extent than by hydrazine or vitamin C.[47] While the thermal reduction does produce a material which is conductive it is extremely defective, and only at temperatures of 1000°C to 2000°C does crystallite size increase significantly as GO becomes completely carbonized.[46] As a result of the defective nature of rGO produced from thermal reduction the surface area shows a marked increase from rGO prepared by hydrazine reduction, 466 m^2/g compared to 600-700 m^2/g.[33,48]

3.3 Chemical Vapor Deposition

Chemical Vapor Deposition (CVD) of graphene produces a material with properties closest to that of mechanically exfoliated graphite, such as the scotch tape method. However, unlike mechanically exfoliated graphene CVD graphene can be made available with much larger surface areas and the most state of the art production being available on roll-to-roll scale. Graphene prepared by CVD is in large part free of functional groups and major basal plane defects making it particularly useful in electronic applications where a pristine surface is crucial.

CVD is the process by which a gaseous reactant, or reactants, adsorb onto a chosen substrate and react to form a solid film of product. The preparation of graphene by CVD is considered a bottom-up method. The choice of substrate and carbon source reactants are important for the process to proceed efficiently, and in fact the substrate can act as a growth catalyst for graphene.[49] Reactant gasses are broadly hydrocarbons such as methane, acetylene, and ethylene diluted in molecular hydrogen.[49] The basic workflow for graphene CVD is that a substrate of choice, typically copper or nickel, is sealed in a CVD reactor chamber followed by the release of the desired hydrocarbon gas which is activated by heat, or some other method, thus producing radical carbon species which then favorably adsorb onto the substrate at which the carbon radicals react with one another to form a layer of graphene.[49] All CVD preparations have their own unique gas flow rates, heating or cooling of substrates, temperature and other process conditions and controls broadly affecting the

outcome of the grown graphene.[49] Qualities such as roughness, crystallinity, domain size, thickness among others are all determined by different process and substrate qualities.[49]

One drawback to this method is that the growth substrate is seldom the substrate of interest in fabricating graphene-based devices. For nickel and copper substrates the substrate is chemically etched and transferred onto the substrate or device of interest. The process of transferring graphene from a growth substrate introduces the possibility of damaging graphene and negatively impacting its most desirable qualities.[50] One method to avoid this issue, in this case applied to roll-to-roll CVD graphene on copper, is to laminate the entire growth substrate once CVD is complete and the delamination produces CVD graphene affixed to a flexible polymer substrate.[50] Direct CVD growth onto glass has also been pursued, again cutting out the process of transfer.[51]

3.4 Covalent Bottom-Up Methods

The ability to control graphene sheet size, edge type, and functionality with a high level of molecular precision, as one might envision with synthetic organic chemistry, is desirable. This can be achieved using organic chemistry utilizing the appropriate precursor molecules. However, unlike CVD graphene or GO the size of the material prepared is comparatively limited, producing a discrete material on the order of nanometers, or as often referenced in literature as graphene nanoribbons. The length of graphene nanoribbons can extend to as long as 600 nm.[52]

The typical precursor molecules, or oligomers, are functionalized polyphenylenes, which allows for a wide variety of structural motifs in the final product. There are two primary synthetic pathways for preparing bottom-up GRM's: solution based or on-surface. Solution based is the typical synthetic organic chemistry route of synthesizing the desired products in a solvent mediated environment. The construction of solution based GRM typically takes advantage of Noble or transition metal coupling or cycloaddition reactions to form the polyphenylene backbone which is then graphitized, or forming the conjugated π-network, by intramolecular oxidative dehydrogenation.[53] This particular synthetic pathway has been spearheaded by the research of Klaus Müllen's group.[54] On-surface, or surface-assisted, methods on the other hand have more in

common with the CVD method. In one synthesis method, by Müllen's group in collaboration with Roman Fasel, under ultra high vacuum conditions 10,10'-dibromo-9,9'-bianthryl is deposited on a Au(111) surface by thermal sublimation at 200°C during which the halogenated bianthryl monomer is dehalogenated resulting in a surface-stabilized biradical intermediate which then undergoes a radical addition reaction to form the polymer chain. The deposited substrate is then annealed at 400°C during which a cyclodehydrogenation reaction creates a polymer with an extended π-system.[55] The surface-assisted method has the advantage of avoiding the problem of graphene nanoribbon aggregation, which plagues the solution based method.[52]

4. Nitrogen-Doped GRM's

Heteroatom-doped GRM's are distinct from GRM's which have been chemically functionalized, such as GO or through synthetic means. Heteroatom doping involves the substitution of a carbon atom in the carbon network with a different atom such as nitrogen, for example. Based on the location of the dopant on the periodic table, and its proximity to carbon, many things can be generalized about the quality it will impart on the carbon lattice. Basic qualities of interest in a dopant are atomic size and availability of valence electrons in comparison to carbon.[18] Heteroatoms both provide active sites for reactivity as well as modulate the overall electronic properties of the GRM.[18,56] Heteroatom-doped GRM preparation largely follows the bottom-up and top-down dichotomy. Each preparation method has an impact on the concomitant heteroatom-doped GRM, affecting the atomic concentration of the dopant, specific functionality of the dopant, and the surface qualities. While there are a number of dopants explored by researchers such as nitrogen, boron, sulfur, and phosphorus the intention of this section is to focus solely on nitrogen-doped GRM's.

Nitrogen is a convenient and natural dopant into the graphene lattice due to its similar size in comparison to carbon. The additional valence electron that nitrogen possess impacts the ability of nitrogen-doped GRM's to take part in interesting chemistry. Nitrogen can be substituted into the graphene lattice in three bonding configurations: pyridinic, graphitic, and pyrrolic, (figure 4). All three of these configurations can exist in varying ratios to one another. Graphitic nitrogen

maintains symmetry with the carbon network of graphene and the lone pair is such that it can take part in the extended π-system. Pyrrolic nitrogen is also present in such that the lone pair of electrons take part in the extended π-system. The lone pair of electrons on pyridinic nitrogen on the other hand is not able to take part in the extended π-system meaning it is a Lewis basic site. Characterizing these different nitrogen functionalities in nitrogen-doped GRM samples is challenging, as the regional chemical environment can be a complex combination of the different functionalities.[57]

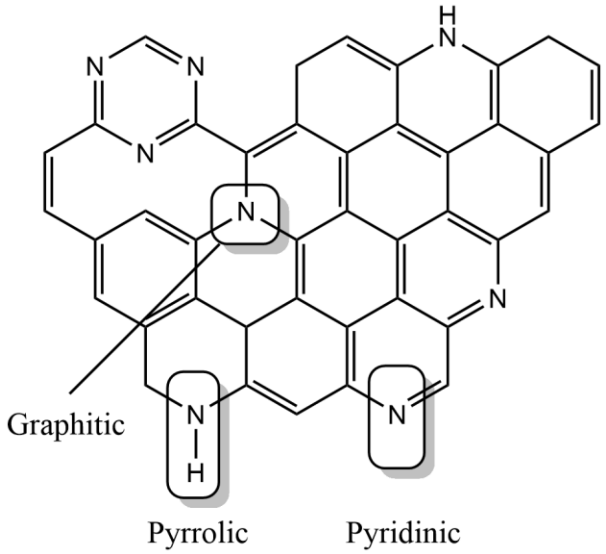

Figure 4. Structure of nitrogen-doped graphene with key nitrogen functionality and heterocycles.

4.1 Preparation Methods of Nitrogen-Doped GRM's

4.1.1 Post-Treatment of GO

In a method proposed by Li et al. 10% ammonia/argon gas flow was used while thermally annealing GO deposited on a SiO_2 substrate at 300 to 500°C.[58] In this process ammonia both reduces and dopes the GO.[58] Nitrogen doping reached a maximum of 5% at an annealing temperature of 500°C with a corresponding oxygen content of ~12%.[58] Based on XPS analysis the predominating form of nitrogen present is pyridinic followed by pyrrolic though the peak

associated with pyrrolic nitrogen shifted as annealing temperature increased to a position which could be indexed to graphitic nitrogen.[58] Li et al. studied the electronic properties of the nitrogen-doped material and determined that proper reduction of oxygen content, by higher annealing temperature, decreases sheet resistance.[58] In a transistor fabricated from N-doped rGO Li et al. reported n-type doping behavior once the device was in a vacuum environment.[58]

Post-treatment of GO also extends to hydrothermal preparation methods. The preparation method is quite simple in that an aqueous dispersion of GO and a nitrogen source is heated in an autoclave at a prescribed time and temperature. The hydrothermal process both dopes and reduces the oxygen functional group the GO.[59] A method involving a hydrazine/ammonia mixture reported by Long et al. showed doping of 5.21, 4.57, 4.09, and 4.01 % at 80, 120, 160, and 200°C, respectively.[59] The oxygen content of the nitrogen-doped rGO at 80,120, 160, and 200°C was 13.13, 13.52, 10.61, 8.61%, respectively.[59] Temperature of the hydrothermal reaction was also shown to affect the morphology, as temperature was increased to a maximum of 200°C the material tended to aggregate.[59] The increase in temperature favors the formation of pyridinic nitrogen, however at lower temperatures pyrrolic nitrogen is the dominating form.[59]

4.1.2 Solvothermal Synthesis

A solvothermal synthesis involving the bottom-up method has been reported by Deng et al. in which carbon tetrachloride and lithium nitride are used as the constituent elements of nitrogen-doped graphene.[60] The method involves heating a solution of lithium nitride in carbon tetrachloride in an autoclave to 250°C.[60] This particular solvothermal method results in halogenation and oxidation of the resultant doped-graphene with chlorine content of 2.7% and oxygen of 3.7%.[60] Based on XPS analysis nitrogen content is 4.0% and according to peak deconvolution graphitic nitrogen is favored followed by pyrrolic and pyridinic nitrogen.[60] Deng et al. proposed that the free-standing nitrogen-doped graphene are formed from dichlorocarbene, ethylene, and imines coupling and dechlorinating carbon tetrachloride into small domains of nitrogen containing sp^2 hybridized carbon, which then assemble into larger sheets.[60] Deng et al.

used scanning tunneling microscopy to image the structural perturbation on the graphene sheet which was corroborated by a density field theory simulated nitrogen-doped graphene structure.[60]

4.1.3 Nitrogen Doping by CVD

CVD synthesis methods have also been applied to preparing nitrogen-doped material. The preparation method does not differ greatly from what is outlined in a typical graphene CVD preparation, namely a copper or nickel substrate heated under a flow of methane/argon/hydrogen gas mixture. The two most cited papers offer a very similar preparation method to one another both utilizing a mix of hydrocarbons, hydrogen, argon, and ammonia utilizing copper and nickel substrates, respectively.[61,62] Qu et al. prepared CVD grown nitrogen-doped graphene on a nickel sputter-coated SiO_2 substrate.[62] The nickel-coated substrate was then heated in a quartz tube furnace and then exposed to an ammonia/methane/hydrogen/argon gas mixture to grow the nitrogen-doped graphene followed by an ammonia/hydrogen gas purge and finally removed from heat under protection of argon.[62] X-ray diffraction and Raman spectroscopy showed that the CVD material prepared by Qu et al. was of a high crystalline quality.[62] XPS analysis of the material showed that pyrrolic nitrogen was the dominant form compared to pyridinic nitrogen with a total nitrogen to carbon atomic ratio of ~4% in addition there was no trace of residual CVD growth catalyst nickel present.[62] In a similar preparation proposed by Wei et al. used a copper-based CVD and a reactive gas mixture of just ammonia and methane, though the cool down step was under hydrogen instead of argon as in the Qu et al. method.[61] Characterization of the material prepared by Wei et al. showed that graphitic nitrogen is the predominant form of nitrogen by far with an overall nitrogen concentration of 8.9%.[61] Wei et al. constructed a transistor device using the CVD nitrogen-doped graphene and were able to demonstrate that the material exhibited n-type doping[61]. Both methods produced material varying from 2 to up to 8 layers.[61,62]

4.1.4 Pyrolysis

One often referenced method is the pyrolysis of carbon and nitrogen containing precursors at high temperatures. This particular method produces a material that is of lower quality when compared to CVD producing a defective basal plane. One such preparation by Li et al. involves the pyrolysis of glucose and dicyandiamide at varying mass ratios, dicyandiamide to glucose of 10 to 40, with a two-step programmed heating under nitrogen atmosphere initially at 600°C then ramped to 800°C and finally cooled[63]. Li et al. were able to show that varying hold time on the high temperature step as well as an increase to 900°C altered the structure and doping level of the material[63]. Material with the shorter hold time at 800°C produced a material with 26.8% nitrogen content whereas increasing hold time and temperature reduces the nitrogen content ultimately to 4.3%[63]. By XPS analysis pyridinic nitrogen is the dominant form in the 800°C followed by graphitic nitrogen, which accounts for greater than 10% of nitrogen forms at all temperature levels[63]. Raman analysis reveals a disordered carbon structure with edge defects[63]. Material prepared is in the form of large monoliths, which can be dispersed and exfoliated in a solvent of choice[63]. In another pyrolysis method reported by Yang et al. melamine and L-cysteine, L-alanine, or L-serine are mixed in a 4 to 1 ratio an pyrolyzed under argon atmosphere at a programmed heating of 600°C followed by a higher temperature of 800°C or 1000°C[64]. Yang et al. propose that the thiol present in L-cysteine promotes the formation of thioether groups at roughly 600°C producing a unique pore structure which when preparing analogous material with L-alanine or L-serine is not observed[64]. At elevated temperatures of 800°C and 1000°C the thioether groups are largely gone, less than 1% sulfur, and the nitrogen content is 19.5% and 5.9%, respectively[64]. Based on XPS analysis the dominant nitrogen group is graphitic followed by pyridinic, pyrrolic, and oxidized-nitrogen at 2.80, 1.45, 0.95, and 0.70%, respectively[64].

5. GRM Characterization Methods

Due to the polydispersity of GRM's it makes quantitative understanding of their structure and chemistry difficult; there are none the less methods by which the chemical environment, bonding, surface chemistry, surface morphology, and nanostructure can be elucidated. Nuclear magnetic

resonance (NMR) techniques are largely not used in the study of GRM's, save for some specific instances where unique functionality can be ascertained from proton or carbon NMR. While a host of spectroscopic methods traditionally used in the elucidation of structure and chemistry are employed there are in addition scanning probe and electron microscopy methods, which are used to offer qualitative and quantitative information. With the tandem use of spectroscopic methods and various microscopies a picture of the chemistry and structure of the GRM may be forged.

5.1 Spectroscopic Methods

Fourier transform infrared (FT-IR) spectroscopy is useful for analyzing GO, doped GRM's, and functionalized GRM's. Specifically, graphene itself is almost IR inactive save for weak peaks from carbon-carbon alkene and carbon-hydrogen vibrations as well as adsorbed water. However; due to the nature of GRM's it may be useful to employ attenuated total reflection (ATR) FT-IR, or diffuse reflectance infrared Fourier transform spectroscopy (DRIFTS). The utilization of ATR and DRIFTS are a consequence of the grinding and pressing required for preparing a KBr pellet for typical transmission FT-IR that may not be possible with a specific GRM such as a thin film.

Raman spectroscopy is well suited to studying GRM's as the carbon-carbon alkene network in GRM's is Raman active and additionally provides information regarding the structure of the sheet such as crystallite size, degree of defect, doping, and number of layers.[65] GRM's produce characteristic peaks in Raman spectra allowing for rapid diagnosis of material characteristics. The characteristic peaks of GRM's at ~1580 cm^{-1} and ~1360 cm^{-1} are referred to as D and G peaks, respectively.[66] The D and D' peaks have been shown to be related to defects and edges present in GRM's.[66] Single layer graphene may be identified by the presence of a prominent G peak and a 2D, or G', peak occurring at ~2700 cm^{-1}.[66] The modulation of the 2D peak gives information regarding the number of graphene layers present.[65] The bulk of information about GRM's is gleaned from Raman peak positions, peak ratios, intensities, and line shapes from which carbon hybridization, defect, and crystallite size can be estimated.[65] One often reported metric of Raman spectra of GRM's is the ratio of D and G peak intensity. Raman mapping, or statistical Raman, is a useful method for analyzing GRM's as it is possible to construct an image of the different

qualities (defects, impurity phases, etc) of the GRM under study by scanning an entire area of the material.[67] Peak position and peak ratios have been shown to be dependent upon laser excitation wavelength so in analyzing GRM's and comparing to the wealth of published literature it must be noted what laser wavelength is used.[65] The benefits of Raman spectroscopy is that spectra acquisition is fast and sample preparation is very simple, or unnecessary, and samples are not damaged in the process.

Ultraviolet visible (UV-Vis) spectroscopy has also been useful for studying GRM's. Specifically in the preparation of rGO the UV-Vis spectra produces a red-shift due to the presence of $\pi \rightarrow \pi^*$ transitions from sp^2 hybridized carbon in effectively reduced GO.[38] Carbon quantum dots and other carbon allotropes give characteristic UV-Vis absorbance spectra, such as the diameter of carbon nanotubes gives specific red-shift and absorbance peak maximum.[68] In studying photoluminescent GRM's, such as carbon quantum dots, fluorometry is needed to study their emission spectra.

X-ray photoelectron spectroscopy (XPS) is a versatile method for investigating GRM's surface chemistry, especially those with heteroatom doping and functionalization. The depth of surface analysis by XPS is considered to be approximately 1-10 nm and can determine the presence of elements greater than hydrogen and helium.[69] In many applications structure to property relationships are of a singular importance and as such an accurate appraisal of the chemical states of GRM's is necessary. The information retrieved from the peak binding energy in XPS data gives information about the chemical states and relative composition of atoms in a material.[69] Using high resolution XPS data, applying curve fitting, peak deconvolution, reference material, and referencing literature on the specific materials it is possible to determine the local chemical environment of the atom in a specific peak binding energy range being investigated.[69] The chemical environment can show the oxidation state, nearest-neighbor atom, and hybridization. In the case of doped GRM's this is crucial for showing the chemical state of dopants and quantification of dopants. However, this method makes use of particular assumptions about the homogeneity of the material being studied which at material surfaces may not be the case as such it is important to consider this in assessing insights on chemistry and composition of materials gained from XPS.[69]

5.2 Electron and Scanning Probe Microscopy

Electron microscopy, specifically scanning electron microscopy (SEM) and transmission electron microscopy (TEM) are useful for shedding light on the nanoscale and microscale features of GRM's. While SEM images offer details about material surface topology as the microscopy method is based on secondary electrons ejected by the primary electron beam, TEM images objects by the electrons, which have passed through the sample thus offering images that elucidate what is essentially inside the sample. One perennial example of TEM's use is showing layers in GRM's or multiwalled carbon nanotubes. High resolution TEM images may provide exceptionally detailed information regarding edge states, grain boundaries, and lattice defects in GRM's.[70] Unlike spectroscopic methods like Raman where sample preparation and operation is fast and easy, TEM and SEM on the other hand are demanding in they require an experienced instrument operator and detailed sample preparation.[70]

Scanning probe microscopy, such as atomic force microscopy (AFM) or scanning tunneling microscope (STM), provide insight into the structure and surface morphology of GRM's. While it is possible to estimate the number of layers of GRM from AFM it has been shown that this method is prone to error and the wealth of literature data is inconsistent, going between 0.4 nm and 1.8 nm for the reported thickness according to one analysis of reported findings.[71] STM on the other hand can provide extremely detailed images of the chemical species and structures adsorbed on material surfaces, such that even self-assembly on GRM surfaces can be monitored.[72] In particular STM is employed to offer detailed images of epitaxially or CVD grown graphene giving information about both the crystal orientation of substrate and graphene.[73] While AFM physically probes the surface, STM can give information about local electronic states on GRM surfaces.[74] Unlike spectroscopic methods, STM and AFM are used only to study localized sections of GRM's.

5.3 Other Characterization Methods

Since the field of inquiry into GRM's and their applications is broad and expanding, the demands of characterizing and studying them require a host of methods and listing them all exhaustively is

outside the scope of this thesis. However; a brief overview of some commonly used methods cited in literature will be addressed here. Thermogravimetric analysis (TGA) is one useful method to investigate the presence of different moieties in GRM's as the decomposition temperature is reflective of different kinds of oxygen containing groups or other functionality and the proportion of mass lost during the decomposition process is reflective of relative concentration of the functional group. Determining analytically the presence and concentration of metal contaminants in GRM's is a very important part of researching GRM electrodes for energy applications as even trace metals can cause anomalous electrochemical behavior.[75] One method for quantifying trace metals in GRM samples is inductively coupled plasma atomic emission spectroscopy (ICP-AES), this method is reported widely in literature as the gold standard for determining trace elemental contaminants.[75] Determining specific surface area is another important characteristic of GRM's as many material applications of different GRM's can be conferred from gas adsorption and specific surface area. The method by which gas adsorption and surface area is typically determined is by Brunauer Emmett Teller (BET) isotherm analysis. BET analyzers function by measuring the relative pressure of an adsorbate vapor and the volume adsorbed and using BET isotherm theory it is possible to then calculate the specific surface area of the material under study. BET analysis can also be used to determine if different gas species have a favorable adsorption interaction with GRM's. Performing in situ characterization is an additional method by which different transition states, metastable intermediates, material growth,and chemical states can be monitored as they arise in a reaction vessel or when materials are exposed to specific conditions that are of interest. An example of in situ characterization is the time-resolved XPS and X-ray diffraction (XRD) characterization of graphene grown on different metal alloys or monitoring the electrochemical reduction of GO by FT-IR and Raman spectroscopy.[76,77]

6. Thesis and Outline of Work Conducted in This Study

As it has been discussed the specific methods of preparation and dopant choice broadly impact the qualities of GRM's. The aim of this work is to study the differences between two different preparation methods of nitrogen-doped GRM's and the resultant materials' ability to be utilized as an electrocatalyst for the reduction of 4-nitrophenol (4-NP). These differences can be elucidated

through different characterization methods thus providing a relatively complete picture of the chemistry and nanostructure of the materials prepared. 4-NP serves as a convenient benchmark for studying the differences in two doped GRM's as well as being a real-world analogue of a persistent environmental pollutant. There is a further precedent in literature as well; electrodes modified with nitrogen-doped GRMs for the detection of 4-NP have reported electrocatalytic effects in the results of their research in addition to the ability to detect 4-NP.[78,79] Nitrogen-doped GRM's have also shown to be effective as a heterogenous reagent for reduction of 4-NP.[80] Utilizing this knowledge about the nitrogen-doped GRM's structure and benchmarking them against their performance with undoped material as an electrode material in the reduction of 4-NP it may be possible to infer structure/property to performance.

The two materials prepared herein can be classified broadly as being prepared by a top-down method and a bottom-up method. The top-down method involves the hydrothermal reduction and nitrogen-doping of graphene oxide, or simply hydrothermal nitrogen-doped graphene (H-NG). The bottom-up method involves the pyrolysis and carbonization of nitrogen and carbon-containing molecules in a tube furnace, or simply furnace nitrogen-doped graphene (F-NG). In addition, a sample of honeycomb boron and nitrogen doped carbon (HC-BCN Pune) was received from a University of Turku research partner, the CSIR-National Chemical Laboratory Pune India, will be included for comparison.

The hydrothermal method employed for preparing H-NG is largely based on the work of Zhang et al. in their 2012 paper, "Wet Chemical Synthesis of Nitrogen-Doped Graphene Towards Oxygen Reduction Electrocatalysts Without High-Temperature Pyrolysis".[81] Outlined in the preparation is the use of dicyandiamide as the molecular source of nitrogen to be incorporated into GO which during the hydrothermal treatment becomes nitrogen-doped rGO **1**, (scheme 2).

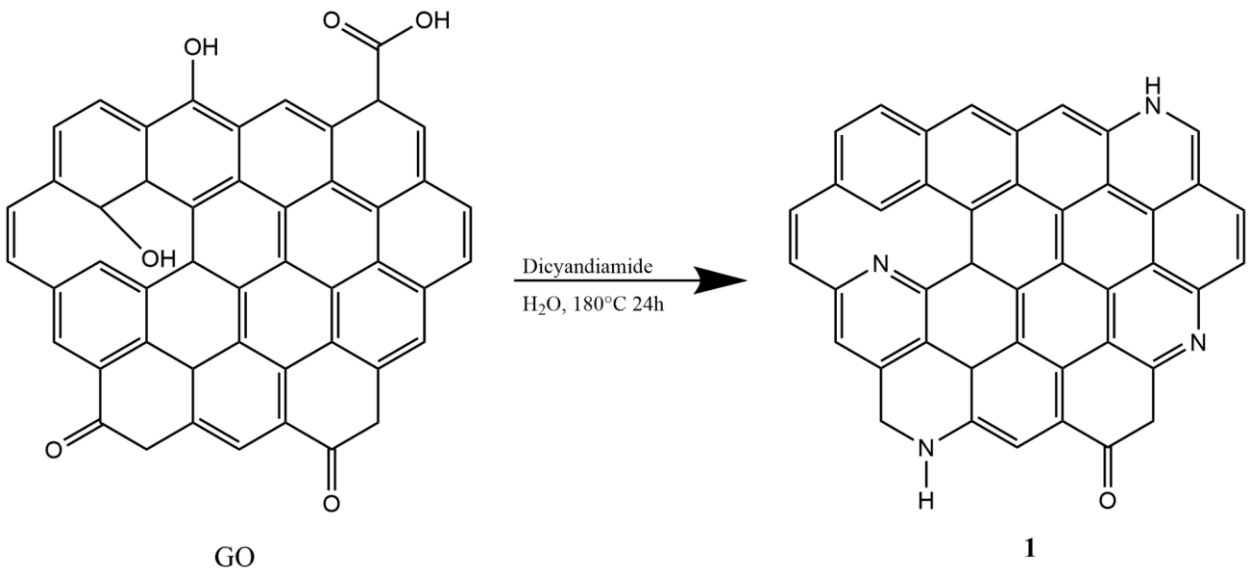

GO **1**

Scheme 2. Chemical synthesis of hydrothermal nitrogen-doped rGO.

The thermal pyrolysis synthesis route for F-NG is one based work done by Liu et al. in their 2018 paper, "Identifying Active Sites of Nitrogen-Doped Carbon Materials for the CO_2 Reduction Reaction".[82] The preparation is based on the pyrolysis and carbonization of melamine and β-alanine in a tube furnace under an inert atmosphere producing nitrogen-doped graphene **2**, (scheme 3).

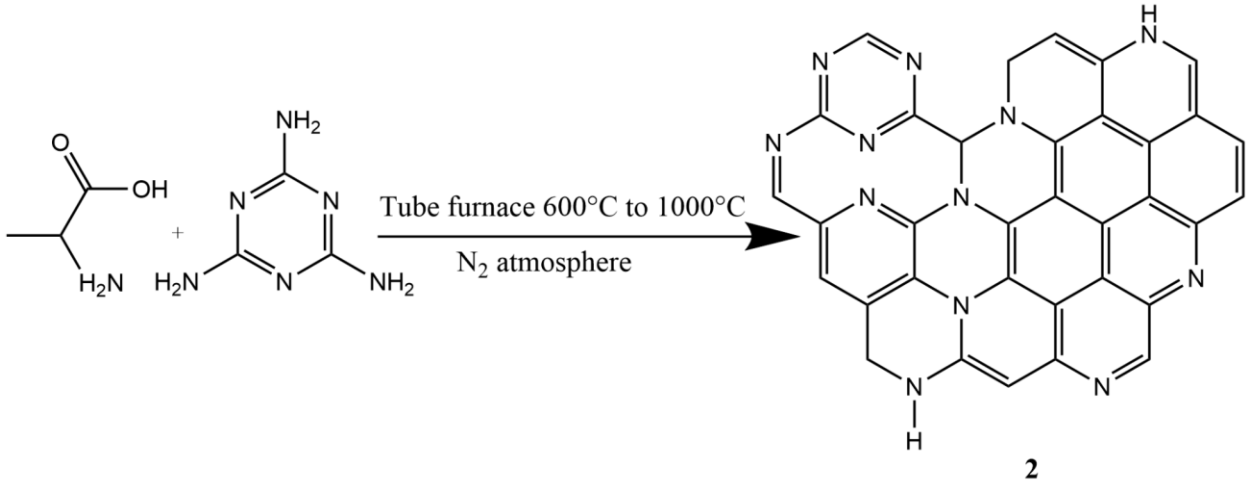

2

Scheme 3. Chemical synthesis of nitrogen-doped graphene.

The prepared materials will then be characterized by FT-IR, Raman, XPS, AFM, SEM. The electrochemical qualities of these materials will be studied by cyclic voltammetry in their effectiveness in electrochemical reduction of 4-NP.

7. Experimental Methods and Materials

7.1 GRM Material Synthesis

7.1.1 Materials

GO was prepared by Rahule Yewale and Milla Suominen, in 2019 via a modified Hummers Method and was used without further purification.[32] All chemicals and solvents specified in the following experimental procedures were used as received. The acid digestion bomb used in the hydrothermal synthesis is a teflon-lined Parr Instruments model 4749. The tube furnace used in the pyrolytic synthesis is Carbolite Gero EST 1200.

7.1.2 Hydrothermal Synthesis of Nitrogen-Doped Reduced Graphene Oxide

A clean and dry test tube was charged with 0.8 mL GO solution (5 mg/mL) to this solution 16.8 mg (0.2 mmol) of dicyandiamide was added. The mixture of GO and dicyandiamide was diluted with 3 mL of deionized water followed by sonication for 1.5 hours at a medium sonication setting in a bath sonicator. Once the sonication time had elapsed the GO dicyandiamide solution was transferred into the acid digestion bomb and the test tube was rinsed forward into the acid digestion bomb with 3 2 mL washes of deionized water. The acid digestion bomb was then properly sealed and heated to 180°C in an oven for 24 hours. Once 24 hours had elapsed the acid digestion bomb was removed from the oven and allowed to cool to room temperature under atmospheric conditions. Once the acid digestion bomb was cooled to room temperature it was then unsealed, the appearance of the product were black flakes roughly 1-2 mm in size. The contents of the acid digestion bomb was transferred to a clean centrifuge tube. The product was then centrifuged for

30 minutes at 50000 RPM after which the supernatant liquid was removed with pasteur pipette, such that the solid product concentrated at the bottom of the centrifuge tube was undisturbed, and then collected supernatant liquid was discarded. To the centrifuge tube containing the product approximately 4 mL of deionized water was added and agitated to allow mixing of the product and fresh deionized water. The same regiment of centrifugation and removing of supernatant liquid and replenishing with deionized water was repeated 3 times in total. After the third regiment of centrifugation the supernatant liquid was removed and filled with approximately 4 mL of ethanol and agitated. The centrifuge tube with product and ethanol was then subjected to the same regiment of centrifugation and removal of supernatant liquid and replenishment of ethanol 3 times. After the third regiment of centrifugation the supernatant liquid in the centrifugation tube was removed and filled with approximately 4 mL of 30% v/v HCl and agitated followed by centrifugation at 50000 RPM for 30 minutes. Once the time had elapsed the supernatant layer from the centrifuge tube is removed and replenished with approximately 4 mL of deionized water. The process of centrifuging at the frequency and time stated above and removing the supernatant layer and replenishing with approximately 4 mL of deionized water is repeated until a neutral pH is achieved by testing with pH test strips. After achieving a neutral pH the product was transferred to a clean, dry and tared glass vial in such a manner that the quantity of water needed to accomplish the task is minimal. The wet product was then allowed to dry in a desiccator such that the mass when weighed was stable.

7.1.3 Hydrothermal Synthesis of Reduced Graphene Oxide

A clean and dry test tube was charged with 0.8 mL GO solution (5 mg/mL). The mixture of GO was diluted with 3 mL of deionized water followed by sonication for 1.5 hours at a medium sonication setting in a bath sonicator. Once sonication time had elapsed the GO dicyandiamide solution was transferred to the acid digestion bomb and the test tube is rinsed forward into the acid digestion bomb with 3 times 2 mL washes of deionized water. The acid digestion bomb was then properly sealed and heated to 180°C in an oven for 24 hour. Once 24 hour had elapsed the acid digestion bomb was removed from the oven and allowed to cool to room temperature under atmospheric conditions. Once the acid digestion bomb had cooled to room temperature it was then

unsealed, the appearance of the product, (figure 5), is black flakes roughly 1-2 mm in size. The contents of the acid digestion bomb were transferred to a clean centrifuge tube. The product was then centrifuged for 30 minutes at 50000 RPM after which the supernatant liquid was removed with pasteur pipette such that the solid product concentrated at the bottom of the centrifuge tube was undisturbed and the collected supernatant liquid was discarded. To the centrifuge tube containing the product approximately 4 mL of deionized water was added and agitated to allow mixing of the product and fresh deionized water. The same regiment of centrifugation and removing of supernatant liquid and replenishing with deionized water was repeated 3 times in total. After the third regiment of centrifugation the supernatant liquid was removed and filled with approximately 4 mL of ethanol and agitated. The centrifuge tube with product and ethanol was then subjected to the same regiment of centrifugation and removal of supernatant liquid and replenishment of ethanol 3 times. After the third regiment of centrifugation the supernatant liquid in the centrifugation tube was removed and filled with approximately 4 mL of 30% v/v HCl and agitated followed by centrifugation at 50000 RPM for 30 minutes. Once the time had elapsed the supernatant layer from the centrifuge tube was removed and replenished with approximately 4 mL of deionized water. The process of centrifuging at the frequency and time stated above and removing the supernatant layer and replenishing with approximately 4 mL of deionized water was repeated until a neutral pH was achieved by testing with pH test strips. After achieving a neutral pH the product was transferred to a clean, dry and tared glass vial. The wet product was then allowed to dry in a desiccator such that the mass when weighed was stable.

Figure 5. A vial of H-NG reaction mixture.

7.1.4 Pyrolytic Synthesis of Nitrogen-Doped Graphene-like Material

In a clean and dry mortar and pestle 2.52 g (20 mmol) melamine and 0.45 g (5 mmol) β-alanine were combined and thoroughly mixed and pulverized in such a manner as to bring both chemicals into intimate contact. Once thoroughly mixed the mixture was then transferred to an alumina boat and placed in a furnace. The furnace was fired under a nitrogen atmosphere using the following time-temperature profile: ramp of 2.5C/min to 600°C and held at 600°C for 2 hours followed by a ramp of 2°C/min to 1000°C and held at 1000°C for 2 hours after which the furnace was turned off and allowed to cool to room temperature. The product of the pyrolysis and carbonization, a black flakey solid in appearance, was transferred from the alumina boat to a büchner funnel fitted with a tared paper filter, see image 2. The product was washed with deionized water, ethanol, and 16% v/v HCl followed by enough deionized water was neutral according to pH paper. The wet product

and filter was placed into a vacuum oven at 50°C and held at ~17 mbar for 24 hours. The dried product, (figure 6), was then stored in a desiccator.

Figure 6. Petri dish containing F-NG atop a sheet of filter paper.

7.2 Preparation of Electrodes and Electrochemical Experiments

7.2.1 Materials

The working electrode used was a Edaq model ETO51 with a 3 mm diameter glassy carbon disk in a PEEK body with a 6 mm outer diameter. Polishing pads used was a DP-Nap by Struers and the polishing paste used was Struers DP-Paste P using particle sizes of 0.25 µm, 1 µm, 3 µm, and 6 µm. Tetrabutylammonium hexafluorophosphate ($TBAPF_6$) was purified by drying in vacuum at 17 mbar at a temperature of 70°C for 24 hours and stored in a desiccator once purified. 4-NP was

recrystallized from hot deionized water and stored in a desiccator. The aforementioned GCE was employed as a working electrode, Pt wire as counter electrode, and Ag/AgCl wire as reference electrode. The Ag/AgCl electrode was standardized against a ferrocene couple. Cyclic voltammograms were made with a Autolab PGSTAT101 potentiostat with Nova 2 software. The single compartment three-electrode electrochemical cell was fashioned from an 18 mL glass vial with a fill line marked at 7.5 mL, allowing for sufficient submersion of the electrodes. Prior to conducting measurements, the electrochemical cell charged with electrolyte solution was purged by bubbling N_2 through the solution. All measurements were made at scan rates of 25, 50, 75, and 100 mV/s with a potential window of 0.00 V to 2.00 V. A solution of a 0.1 M solution of purified $TBAPF_6$ was prepared in acetonitrile from which a 1 mM solution of 4-NP was prepared, thus producing a 1 mM 4-NP solution in 0.1M $TBAPF_6$ acetonitrile (ACN).

7.2.2 Polishing and Cleaning Method of Glassy Carbon Electrode

The glassy carbon electrode (GCE) was polished by applying polishing paste onto a polishing pad adhered to a petri dish to which a small amount of ethanol was added to produce a slurry of polishing paste. The electrode was polished by rubbing the electrode surface in a figure-eight motion on the polishing pad in the polishing paste slurry for 40 seconds, this process was repeated for each polishing paste particle size starting from the largest particle size (1 μm) to the smallest (0.25 μm). Upon completion of the polishing process the GCE was rinsed with deionized water and ethanol to remove visible polish slurry. The polished tip of the GCE was submerged in a vessel containing deionized water and sonicated in a bath sonicator for 10 minutes. Once the 10 minutes had elapsed the polished tip of the GCE was submerged in a vessel containing ethanol and sonicated for 10 minutes in a bath sonicator. Once the 10 minutes had elapsed the polished top of the electrode was rinsed with ethanol and dried with a 20 second burst of hot air from a hot air gun. The clean and dry polished GCE was then visually inspected.

7.2.3 Preparation of the GRM Dispersion

A 1 mg/mL dispersion of products was prepared by weighing out the dry product in a sample vial and filling with the correct volume to achieve 1 mg/mL. To aid in exfoliation and dispersion large pieces were broken up with a clean and dry glass stir rod. The sample vials were sealed with clean and dry teflon caps and sonicated in a bath sonicator, the bath was cooled with an iced-filled Erlenmeyer flask such that the temperature was kept in the range of 25-32°C. The sample vials were sonicated until it appeared that there were no longer solids on the bottom of the vials.

7.2.4 Drop-Casting of Material onto Glassy Carbon Electrode

The material to be applied to the GCE was sonicated for 10 minutes, making sure that that material is properly dispersed once the time had elapsed in which more sonication is necessary. A freshly cleaned and polished GCE, as outlined above, was immobilized onto a ring stand clamp such that the GCE is facing-up and level. To the GCE 5 coats of 5 μL of the GRM dispersion was drop-cast onto the electrode, after each drop-cast coating the solvent was allowed to dry which was assisted by the use of a high-wattage lamp shown onto the electrode surface.

7.2.5 Electrochemical Measurements in Blank and 4-Nitrophenol Solution

Blank measurements were collected of an unmodified GCE and modified with the different materials prepared according to the aforementioned procedure. Prior to filling the cell the Pt wire was cleaned by flame torch such that it glowed red along the length that would be submerged in the electrolyte solution in addition the Ag/AgCl electrode was rinsed with deionized water and the electrolyte solution to be used in the measurement. The blank measurement consisted of filling the electrochemical cell to the 7.5 mL fill line with electrolyte solution followed by N_2 purging and finally collecting cyclic voltammograms. Measurement of the unmodified and modified GCE in a solution of 1 mM 4-NP 0.1 M $TBAPF_6$ ACN was conducted using the same protocol as mentioned above.

7.3 Sample Preparation and Methods for Material Characterization

7.3.2 FT-IR

FT-IR spectra was collected with an ATR accessory by drop-casting the material onto the analysis crystal on the ATR accessory or placing the dry powder of the material onto the ATR analysis crystal. Spectral assignments were made with the aid of G. Socrates, "Infrared and Raman Characteristic Group Frequencies: Tables and Charts".[83]

7.3.3 Raman

Samples were prepared by drop-casting 30 μL of the prepared materials onto a stainless steel sample stage. Prior to drop-casting the prepared material dispersed in ethanol was sonicated for 30 minutes, or until the material was well dispersed in the solvent. The Raman laser wavelength used for all samples was 532 nm. The peak ratios were calculated from their respective integrated peak areas from curve-fitting using Renishaw WiRE software.

7.3.4 XPS

The material synthesized and graphene oxide starting material were either drop-cast onto a silicon substrate or analyzed as a powder. The silicon substrate was cleaned by an RCA method by first boiling in a 5:1:1 (H_2O: 30% NH_3OH: 30% H_2O_2) solution for 10 minutes followed by a second cleaning solution in a boiling 6:1:1 (H_2O: 37% HCl: 30% H_2O_2) for 10 minutes and finally thoroughly rinsed with ethanol and placed in a desiccator for storage. Prior to drop-casting the cleaned and dry silicon substrate was plasma cleaned with oxygen plasma for 5 minutes. The substrates were coated by drop casting promptly following plasma cleaning. Each substrate was coated with 3 10 μL coats of a 1mg/mL dispersion in ethanol of the material synthesized. Following each coat the substrate was annealed on a 80°C hot plate until the solvent was visibly evaporated. XPS spectra were collected by Dr. Sari Granroth of the University of Turku Materials Research

Laboratory. The XPS spectra was deconvoluted and analyzed with Avantage software with the assistance of Lauri Marttila.

7.3.5 SEM

Material for SEM analysis was prepared by drop-casting a diluted, 0.5 mg/mL, dispersion in ethanol of the materials prepared. The substrate, a silicon wafer, was prepared by 5 minute sonication and rinsing in deionized water, ethanol, and acetone. Each silicon substrate received 3 1 μL coats of freshly sonicated ethanol dispersion of material prepared, prior to an additional coat the solvent was allowed to evaporate.

7.3.6 AFM

A 0.1mg/mL dispersion in ethanol of the materials prepared was made. A longer period of sonication to prepare the dispersion was used than in preparing the material for SEM. The substrate was RCA and oxygen plasma cleaned silicon wafers. Each clean silicon wafer received 3 times 3 μL drops of freshly sonicated dispersed material allowing the solvent to evaporate between aliquots.

8. Results and Discussion

8.1 Elemental and Functional Group Composition of GRM's

The FT-IR spectra, (figure 7), of stock GO show a diagnostic broad and strong peak at ~3200 cm^{-1}, indicating the presence of hydroxyl groups, which by comparison is not present in the rGO, H-NG, F-NG, and HC-BCN Pune material.[83] The other peaks of interest in the GO FT-IR spectra are those of the conjugated cyclic alkenes, carbonyl groups, and ester or aryl oxygen groups occurring at 1620,1718, and 1033 cm^{-1}, respectively.[83] The spectra of the rGO as well as the H-NG both

show the appearance of a new peak, 760 cm^{-1}, which can be attributed to trisubstituted alkenes.[83] The appearance of the trisubstituted alkene and the disappearance of the broad and strong hydroxyl peak at ~3200 cm^{-1} in the FT-IR spectra of rGO and H-NG suggests the successful reduction of a significant portion of the oxygen-bearing functional groups. The peak at 1033 cm^{-1} is also reduced in size considerably in the hydrothermally reduced materials, which reveals a peak at 1225 cm^{-1} attributable to C-O aryl or ether stretching.[83] The rGO shows a weak peak at 1718 cm^{-1}, identified as carbonyl group stretching, however in the H-NG this peak is not present.[83] The disappearance of the carbonyl peak suggests the possibility of the formation of imines in a 1,2-addition at a carbonyl carbon by dicyandiamide. The FT-IR spectra does not adequately elucidate the presence of C-N bonds in the hydrothermally prepared material. The alkene and carbonyl peaks, 1577 cm^{-1} and 1718 cm^{-1} respectively, of the H-NG are slightly shifted from GO starting material. This shift in the peak position has been attributed to both increase in concentration of sp^2 carbon, due to reduction of oxygen functional groups.[84,85]

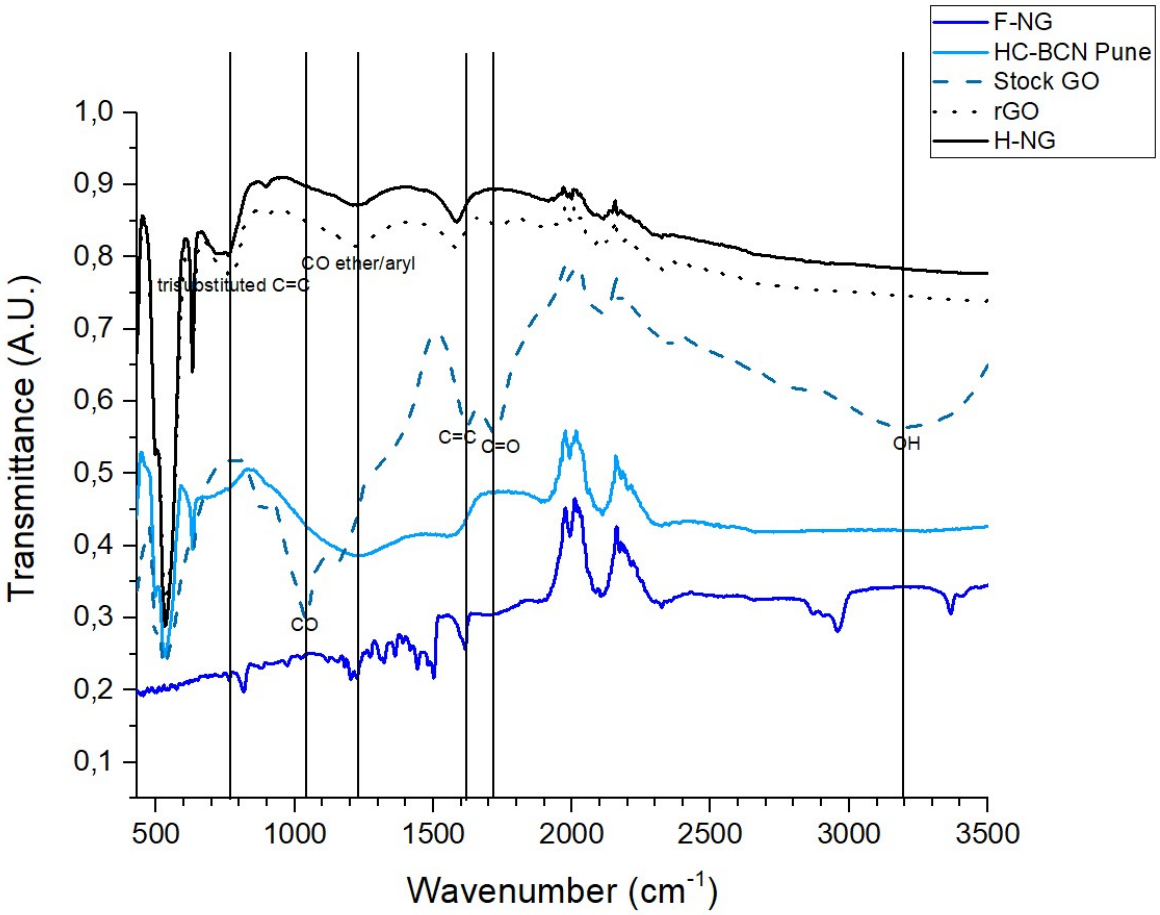

Figure 7. FT-IR spectra of F-NG, HC-BCN Pune, stock GO, rGO, and H-NG. Through lines in the figure correspond to prominent functional groups as labeled in the figure.

The FT-IR spectra of F-NG differs from that of H-NG. One key peak present at 816 cm^{-1} is indicative of carbon-nitrogen stretching of nitrogen-heterocycles such as triazine groups.[83,86] In addition the peaks present from 1203 cm^{-1} to 1501 cm^{-1} are also associated with nitrogen-heterocycles.[86] This can be explained by the use of melamine as precursor material. Melamine undergoes a polycondensation reaction at temperatures in excess of 300°C forming networks of triazine, or graphitic carbon nitride.[87] The peak at 1613 cm^{-1} is ambiguous in that it could be attributed to conjugated alkene stretching or to N-H bending.[83] The peak at 2957 cm^{-1} is associated with C-H bonds in aliphatic compounds.[83] The peak at 3366 cm^{-1}, which could be attributed to symmetric and asymmetric stretching of NH_2 though this assignment is complicated by the fact these peaks are not broad as is often associated with N-H vibrations.[83] The presence of a strong fingerprint peak at 529 cm^{-1} which is a common feature for all of the materials save for the F-NG suggests that there is a fundamental difference in composition in F-NG. This fingerprint region feature can be assigned to trisubstituted alkenes.[83]

FT-IR Spectra of HC-BCN-Pune lacks many distinct peaks for easy assignment of functionality. Though the discernable features in the HC-BCN-Pune FT-IR spectra are all shared in common with the hydrothermally prepared materials, including a strong fingerprint peak at 529 cm^{-1}. The two broad breaks at 1225 cm^{-1} and 1577 cm^{-1} can be associated with carbon-oxygen aryl or ether stretching and cyclic alkenes.[83] A medium peak located at 760 cm^{-1} can be assigned to trisubstituted alkenes.[83]

The ultimate benchmark of determining the successful doping and chemical states present in the materials studied is by XPS. The results for the two different synthesis methods conform, in line shape and peak locations, to the literature sources the synthetic methods were based upon. Comparing the elemental quantification reported in atomic percent (at.%), see table 1, of the materials as synthesized and the literature values the hydrothermally prepared method produced a material with lower percent nitrogen than cited in literature, 5.35% versus the reported 7.78% in literature.[81] In the case of the furnace method the reverse is observed: the prepared material has a

higher percentage of nitrogen than anticipated, 9.25% versus the literature reported 5.40%.[64,82] In the case of material prepared in the furnace, one possible reason for the higher nitrogen content could be that the procedure outlined in the literature uses an argon atmosphere while the adapted procedure reported herein uses a nitrogen atmosphere. Surprisingly HC-BCN Pune appears to have near equal amount of boron and fluorine, the fluorine could be rationalized as being from a boron containing precursor material such as boron trifluoride though this is purely conjecture as the synthetic method for this material in not available.

Material	N (at.%)	C (at.%)	O (at.%)	B (at.%)	F (at.%)
F-NG	9.25	87.99	2.77	0.00	0.00
H-NG	5.35	80.75	13.9	0.00	0.00
rGO	0.00	83.24	16.76	0.00	0.00
HC-BCN Pune	12.09	73.45	7.37	3.67	3.41

Table 1. Elemental composition of the materials prepared as determined by XPS.

The three XPS spectra, and concomitant deconvolutions, show that the chemical environment in the N1s high resolution spectra is different from each other as can be ascertained from the peak positions and line shape, (figure 8). The peak assignments for the materials prepared was in large part in agreement with the literature.[64,81,82] The F-NG and HC-BCN Pune materials share similar peak positions in the deconvoluted peaks, looking at the pyridinic peak assigned to 398.23 eV and 398.29 eV respectively. H-NG on the other hand has two peaks with a pyridinic peak centered at

398.76 eV, in comparison to the other two materials presented.

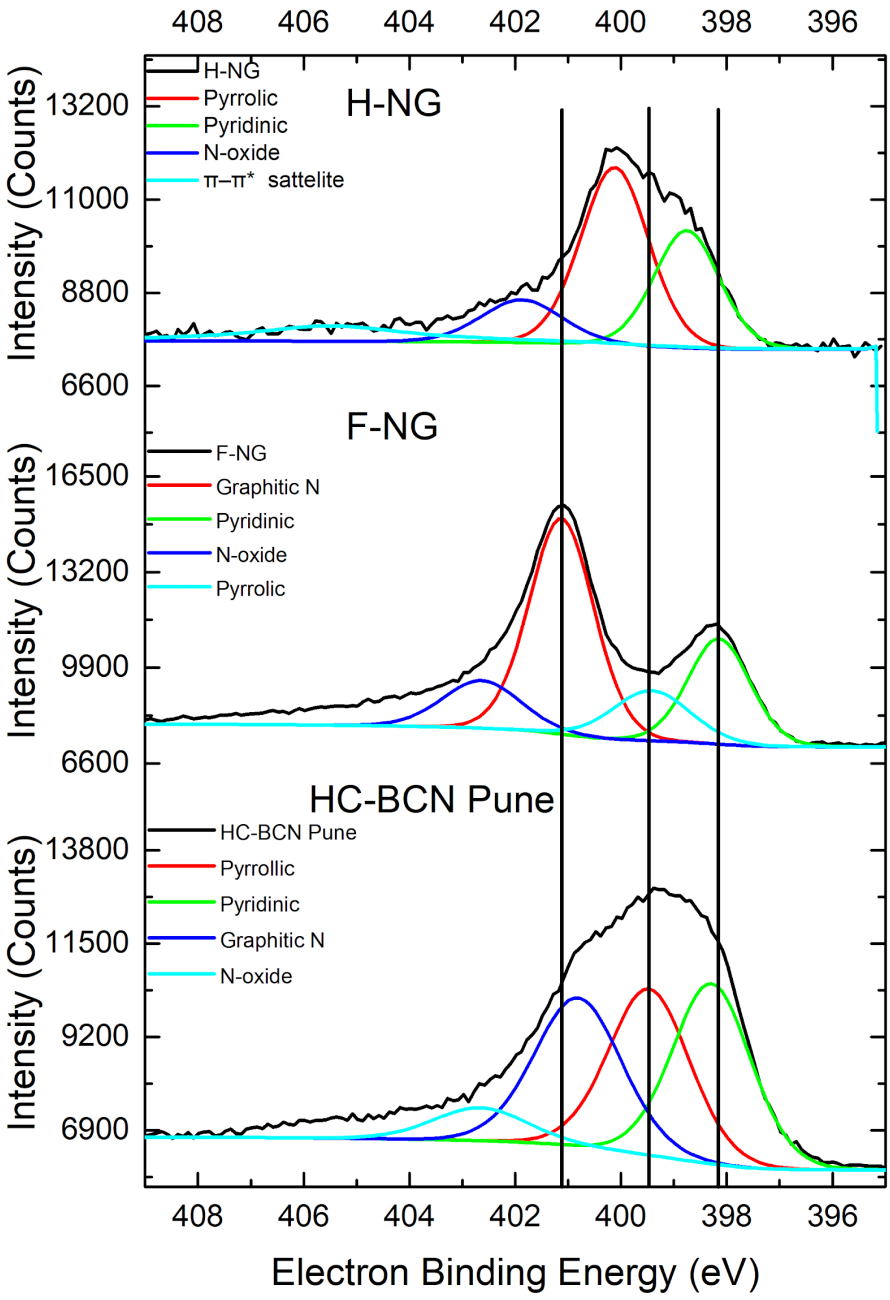

Figure 8. XPS and concomitant curve deconvolutions of the H-NG, F-NG, and HC-BCN Pune materials, through lines are for comparison purposes.

One possible rationalization of the structure of H-NG and F-NG is the location of the nitrogen-containing groups, being either in the basal plane or near or on the edge plane. F-NG deconvolution shows a prominent graphitic nitrogen peak which indicates the presence of nitrogen in the basal plane. The XPS and FT-IR spectra of F-NG can be united in corroborating the presence of triazine or heptazine groups. As the FT-IR spectra of F-NG shows diagnostic peak for triazine, 816 cm^{-1}, indeed the XPS spectra can also substantiate this claim in that the peak binding energy of the pyridinic nitrogen, 398.23 eV, is also associated with the presence of triazine groups.[57] However, from the elemental composition it would seem that the material is not graphitic carbon nitride as the amount if nitrogen would be much greater, closer to 50-60 at.%.[88] From this it can be assumed that in part there is a phase of triazine, or other nitrogen heterocycles, present in the material which is then rendered in the ATR FT-IR while alkene structures are much less active. H-NG conspicuously has no graphitic nitrogen peaks and the nitrogen groups present in the XPS spectra, pyridinic and pyrrolic nitrogen, are indicative of those which are in the edge plane or defect plane. In the H-NG may be conjectured that in the reduction and doping of GO the main functional group being acted upon by dicyandiamide are the carbonyl and carboxylic acid groups found on the edge plane. From the work proffered by Yamada et al. regarding XPS analysis on specific nitrogen-containing functional groups on graphene the binding energy of the H-NG could best be attributed to pyridine functionality on edge planes.[89] A comparable binding energy was also reported in a similar synthesis route, hydrothermal reduction of GO, where pyridinic-like nitrogen was attributed to 298.7 ± 0.3 eV.[59]

8.2 Carbon Structure of GRM's

The Raman spectra of all of the materials prepared, HC-BCN Pune, and GO starting material displayed characteristic peaks at ~1340 cm^{-1} and ~1580 cm^{-1}, reported as D and G peaks respectively, (figure 9). The presence of the D peak is indicative of defects in the sp^2 carbon sheet in the materials prepared and the GO starting material and the G peak is indicative of sp^2 hybridized carbon.[66] One additional quality in common with all of the Raman spectra is the broad and extremely weak 2D peak centered at ~2765 cm^{-1} indicates multi-layer structures.[66] The ratio of D and G peak intensities were in this case used as a means to analyze the progress of the hydrothermal reduction and degree of defect of the GO starting material and the subsequent doping, (table 2).

The change in G peak position of stock GO after hydrothermal and subsequent doping with dicyandiamide is indicative of both doping and disruption of the sp^2 carbon structure, (figure 10).[90] The increase in D/G ratio of the stock GO, rGO, and H-NG is also indicative of the disruption of the sp^2 carbon lattice with the substitution of nitrogen groups and edge defects or other vacancies, (table 2).[90] The qualitative difference in linewidth of the D and G peaks between the materials studied also indicates change in structure of material, in particular the change in crystallite size.[91] The F-NG with the greatest linewidth suggests that it has both a smaller crystallite size in addition the D/G ratio suggests a material with greater fraction of a sp^2 carbon in each crystallite.[91] The line shape of both HC-BCN Pune and F-NG are similar while they differ in D/G ratio this suggests that their crystallite size may be comparable in size but degree of defect and sp^2 carbon ratio is different.[91]

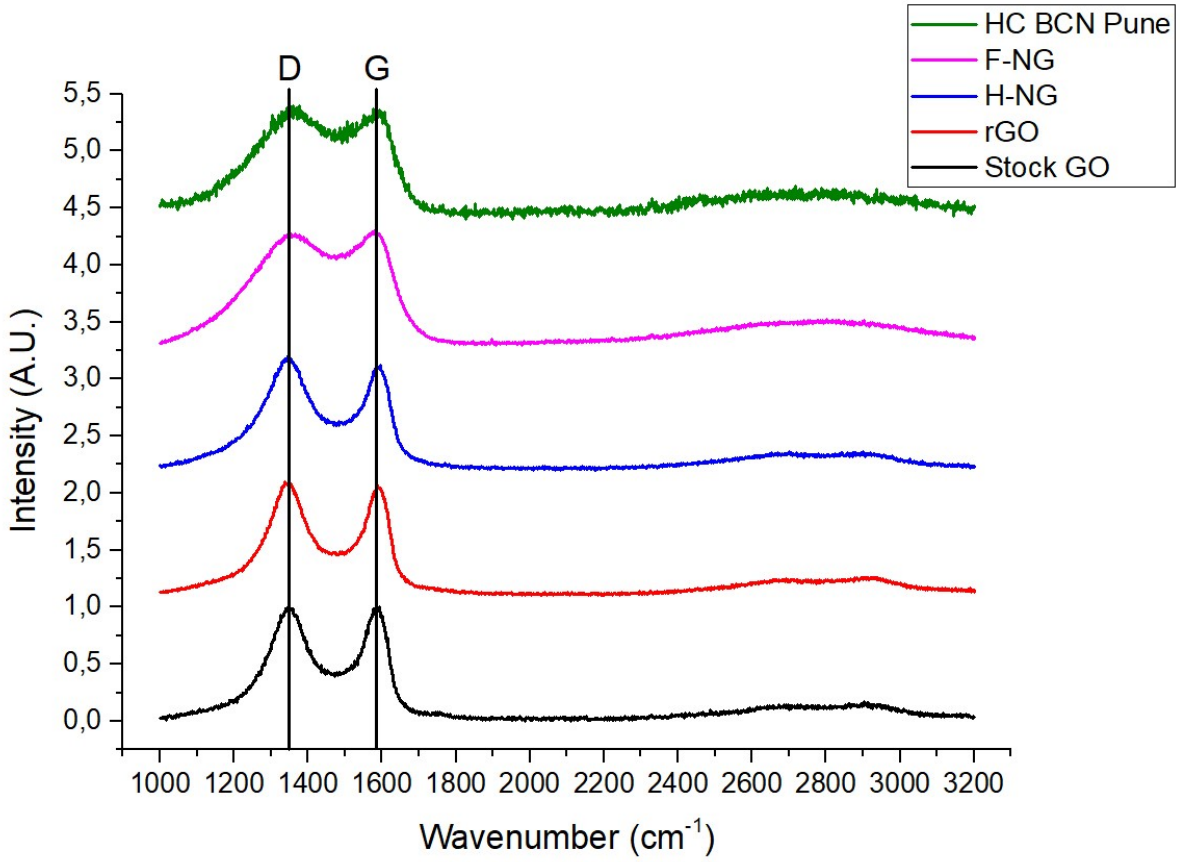

Figure 9. Stacked Raman spectra of HC-BCN Pune, F-NG, H-NG, rGO, and stock GO with through lines through the D and G peak position centered at stock GO spectrum peak positions.

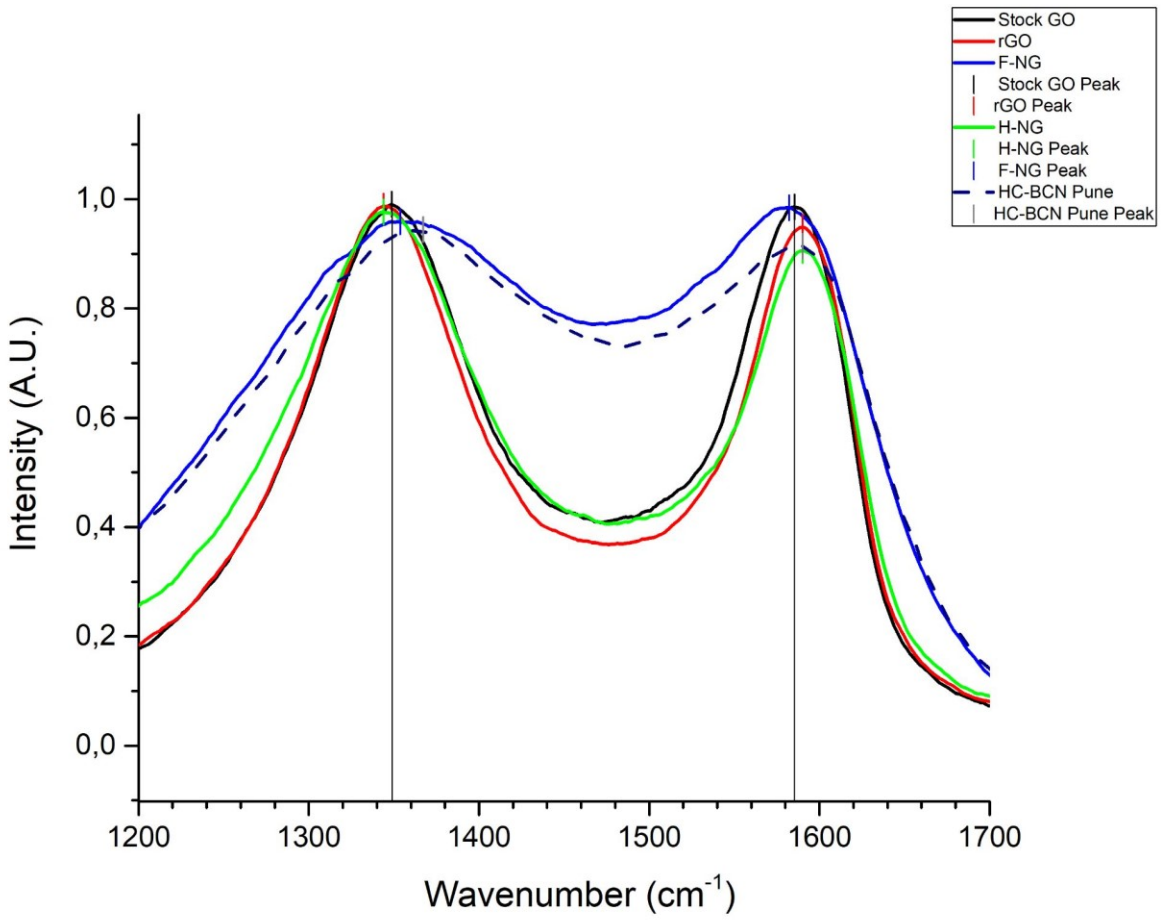

Figure 10. Raman spectra of stock GO, rGO, F-NG, H-NG, and HC-BCN Pune with through lines corresponding to D and G peaks of stock GO.

	Stock GO	rGO	H-NG	F-NG	HC-BCN Pune
D/G	2,10	2,15	2,84	3,61	3,34

Table 2.D/G ratios of stock GO, rGO, H-NG, F-NG, and HC-BCN Pune.

While FT-IR data for the F-NG suggests a material with features of graphitic carbon nitride, the Raman and XPS spectra suggests a material which is indeed a carbon rich material. As such the peak assignment from the FT-IR spectra at 1613 cm^{-1} could then be comfortably assigned to alkene stretching. This diverging data between the two characterization methods may result from the fact that Raman spectroscopy relies upon collecting spectra from the surface of a very fine point, and

the utility of mapping Raman spectra over some fraction of the materials surface may give a greater understanding of the composition of the material. But this further reinforces the hypothesis that the F-NG is inhomogeneous and contains phases ranging from carbon nitride to a carbon rich sp^2 phase.

8.3 Morphology of GRM's

SEM images for rGO, H-NG, F-NG, and HC-BCN Pune are presented below, (figures 11-14). Interpreting the images themselves is complicated by the qualitative nature and monochromatic image produced in SEM. It is my assertion that rGO and H-NG show a difference in appearance that shows more sheet-like structures in rGO and more agglomerated features in the H-NG. In comparison to the rGO and H-NG the F-NG shows a material with clear stacked sheets of material. HC-BCN Pune SEM images show distinct honeycomb-like features in the sub-micrometer size. While the dispersed material was well sonicated prior to drop-casting the SEM images show that the materials do not appear to be well exfoliated, which is especially noticeable in the F-NG material due to the stacked-layers of material in the SEM image. The poor exfoliation may have many reasons from the solvent the material is dispersed in, the intermolecular forces, surface tension, and other factors in the drop-casting process.[17,92] In a detailed analysis of the hydrothermal reduction method Huang et al. observed agglomeration of the resultant rGO material when hydrothermal reaction time is beyond 2 hours, which they attributed to lowering surface energy by stacking of rGO.[44] It has been shown that intercalated water molecules between GO sheets are subject to strong hydrogen bonding thus pulling the sheets together.[93] GO-water hydrogen bonding is a satisfactory rationalization for the sheet stacking observed in the SEM images in light of the synthetic methods used to prepare the materials.

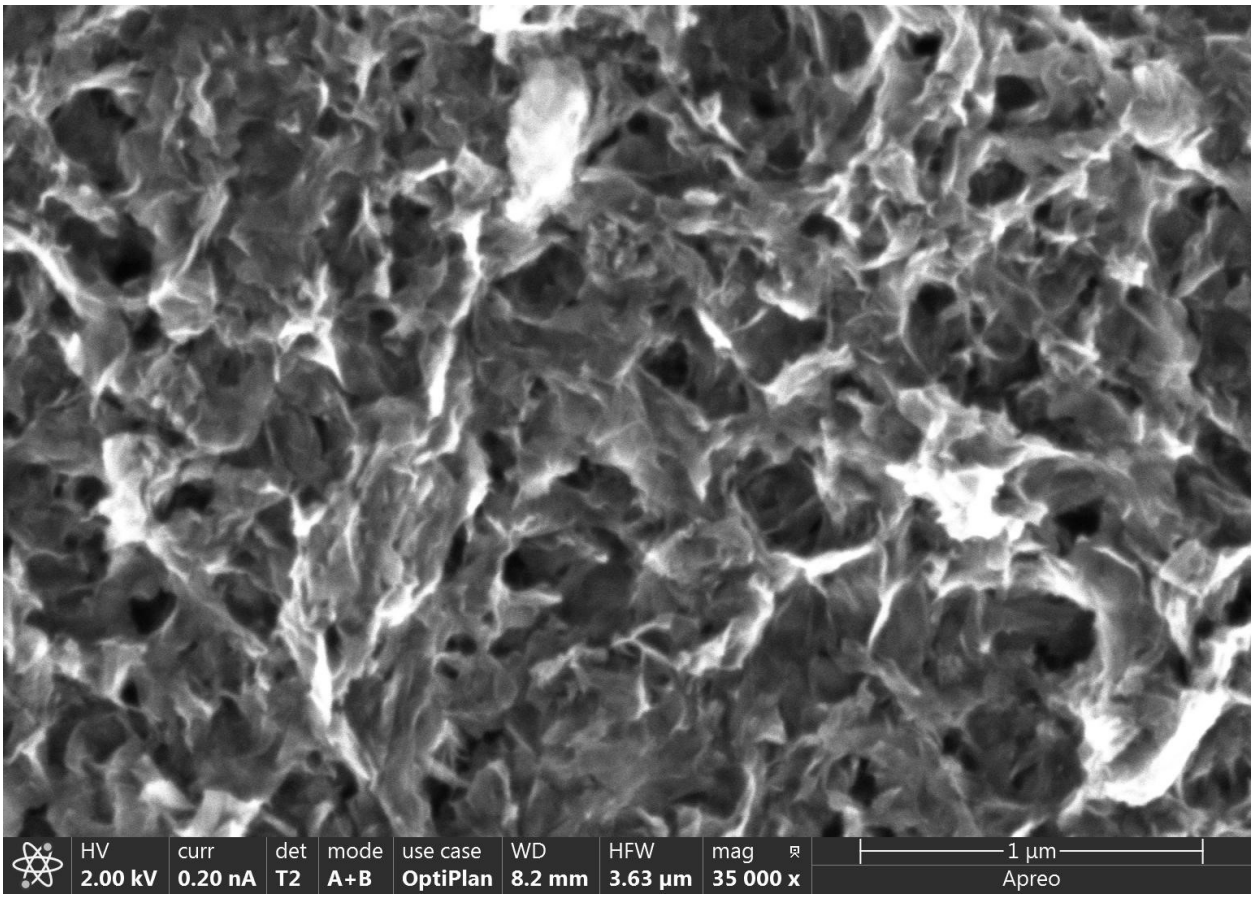

Figure 11. SEM image of rGO.

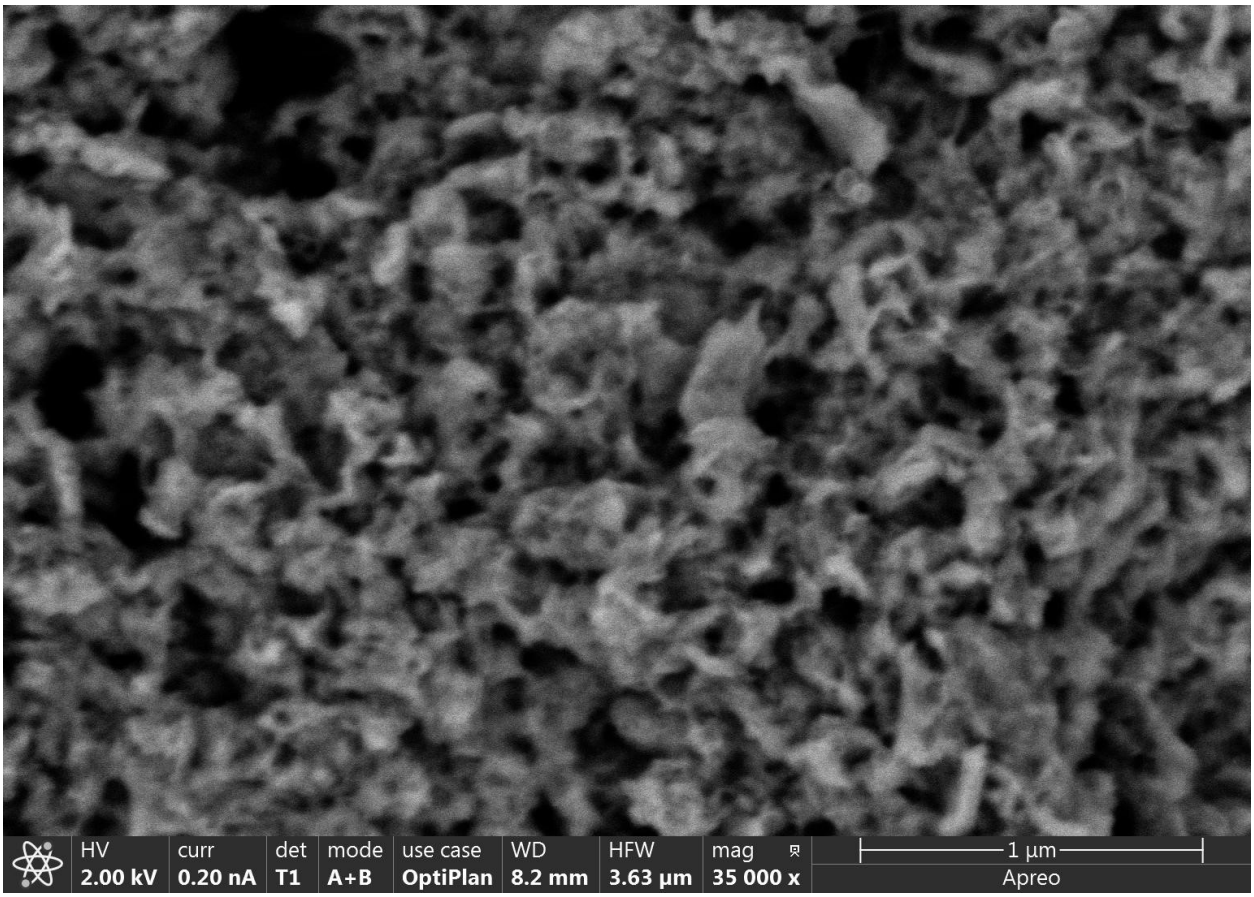

Figure 12. SEM image of H-NG.

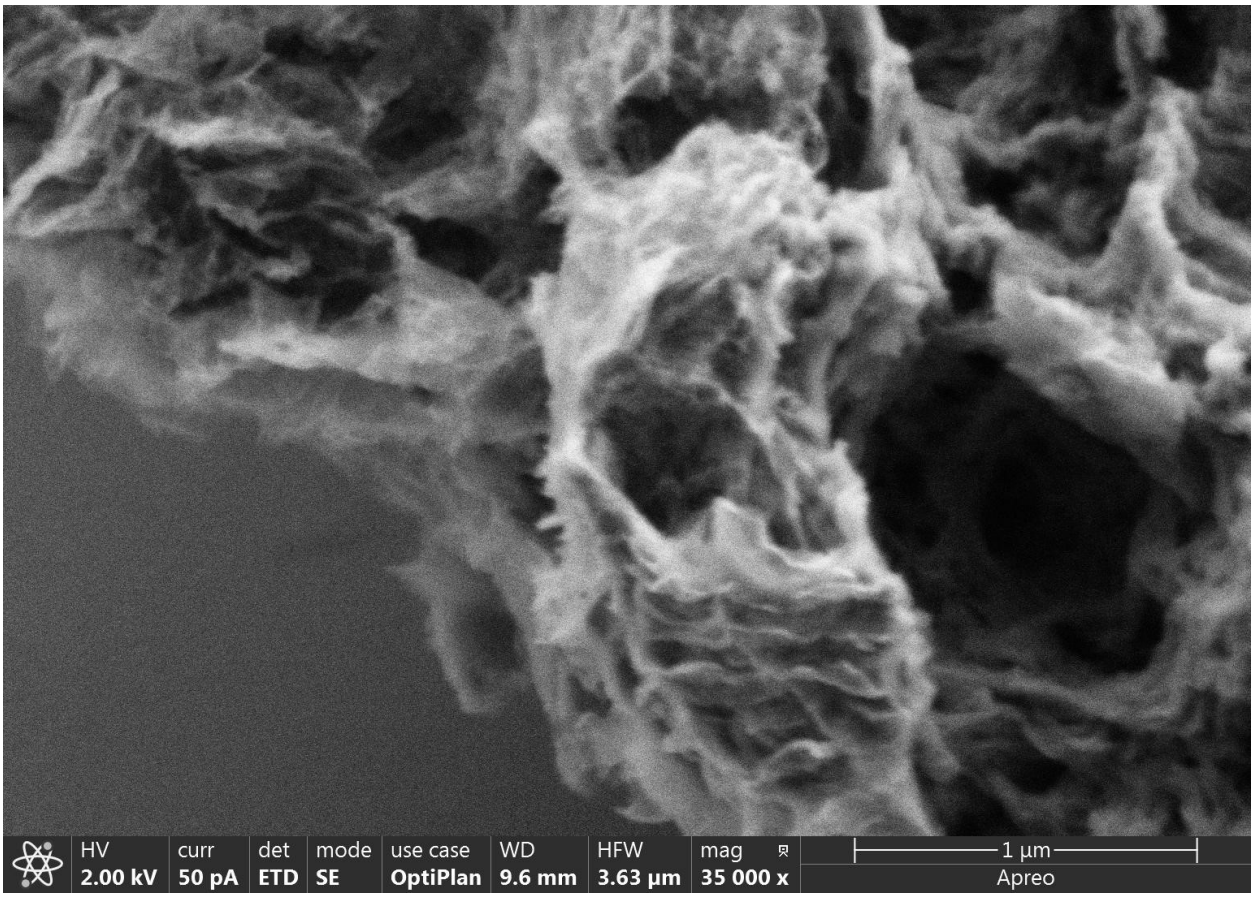

Figure 13. SEM image of F-NG.

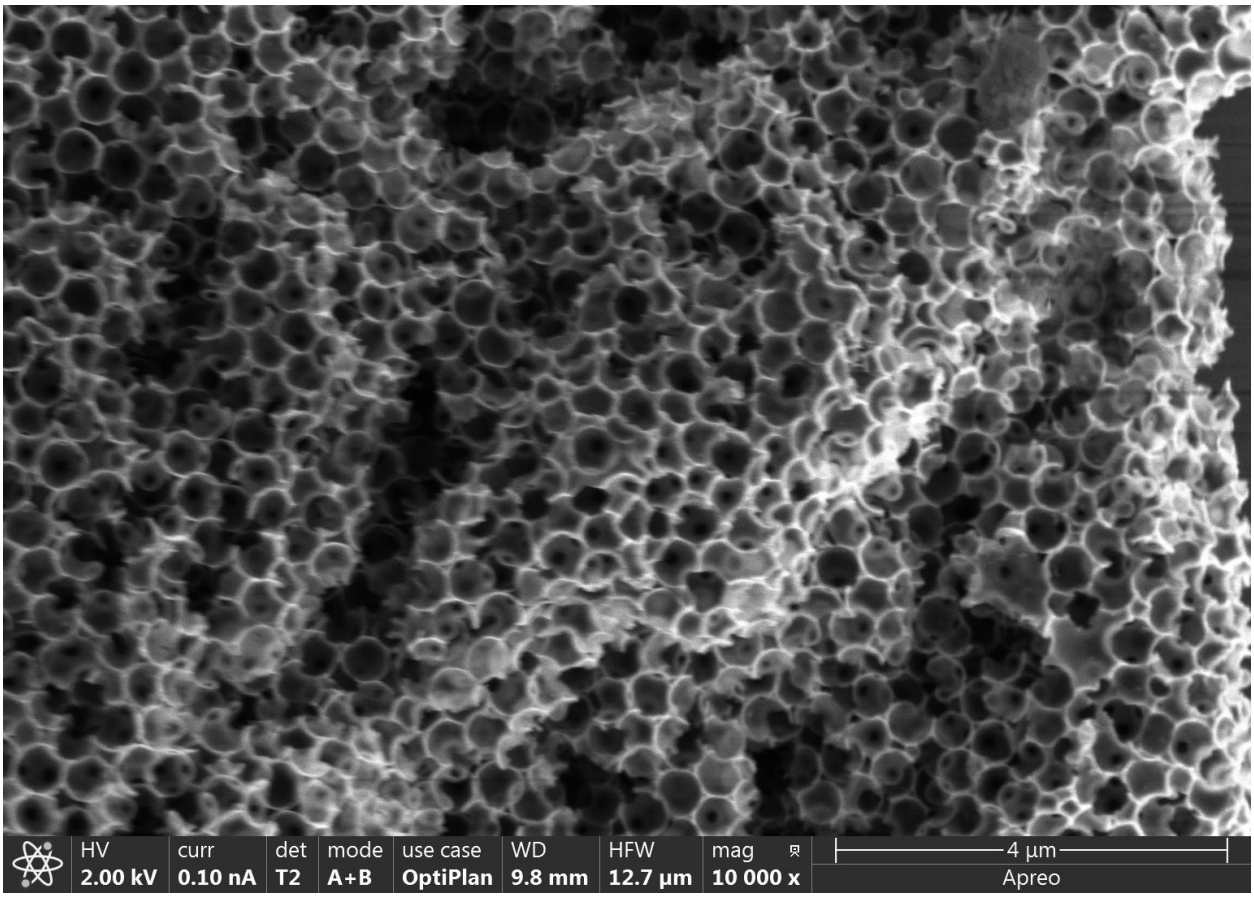

Figure 14. SEM image of HC-BCN Pune.

The AFM images, (figures 15-19), largely corroborate the SEM images above, showing a poorly exfoliated material. The addition of GO to the comparison of the other materials highlights the change in structure after hydrothermal treatment both with and without doping, (figures 15-17). The GO image shows wrinkled sheet-like structure with a height of ~14-16 nm suggesting multiple layers of GO.[71] While the image of rGO shows none of the sheet like qualities, which echo the observations made in the work of Huang et al. in their analysis of the hydrothermal synthetic method for reducing GO.[44] H-NG, F-NG, and HC-BCN Pune are all in a similar height range, between 30 and 40 nm, while rGO appears to be closer to 140 nm. Based on the Raman spectra, SEM, and AFM it can be surmised from the naming and structure rubric outlined in figure 3 that these materials fall decidedly on the GRM spectrum of multilayer carbon materials, such as graphite microplates or graphite oxide.

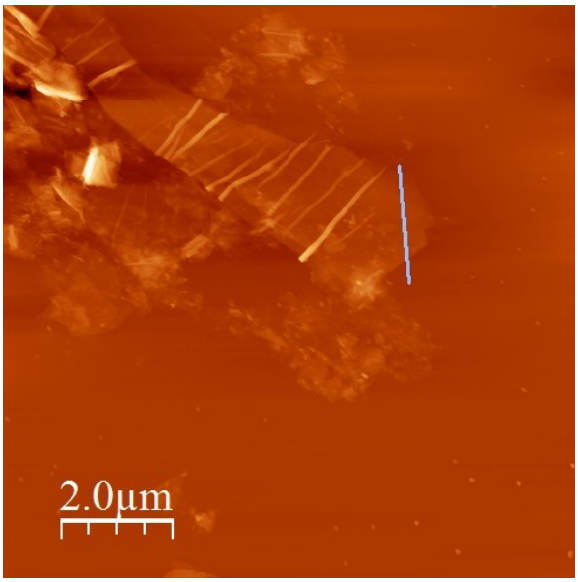

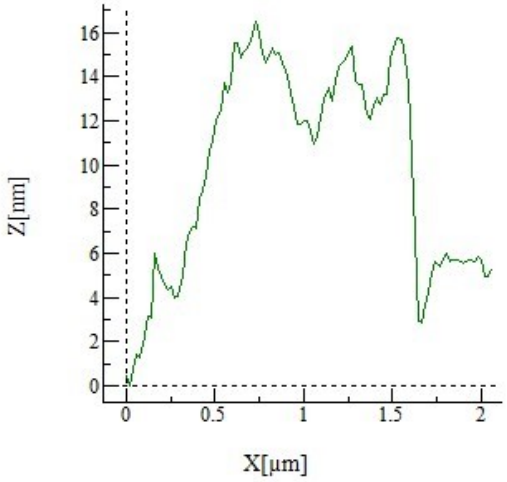

(a) (b)

Figure 15. (a) AFM image of stock GO with inset line indicating area of profile analysis. (b) Corresponding height profile analysis from AFM image.

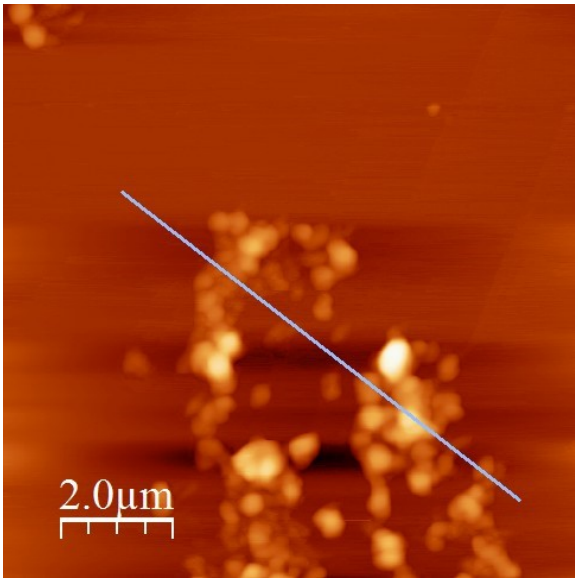

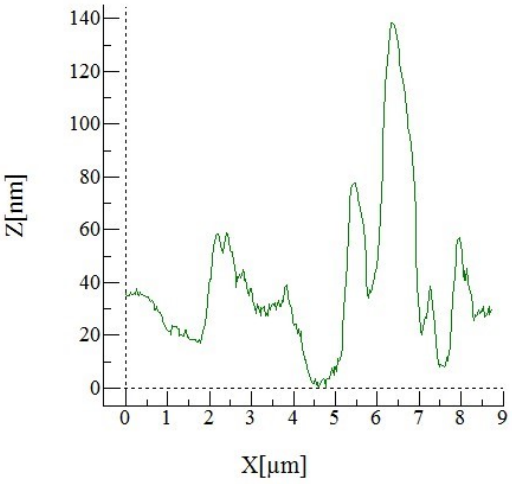

(a) (b)

Figure 16. (a) AFM image of rGO with inset line indicating area of profile analysis. (b) Corresponding height profile analysis from AFM image.

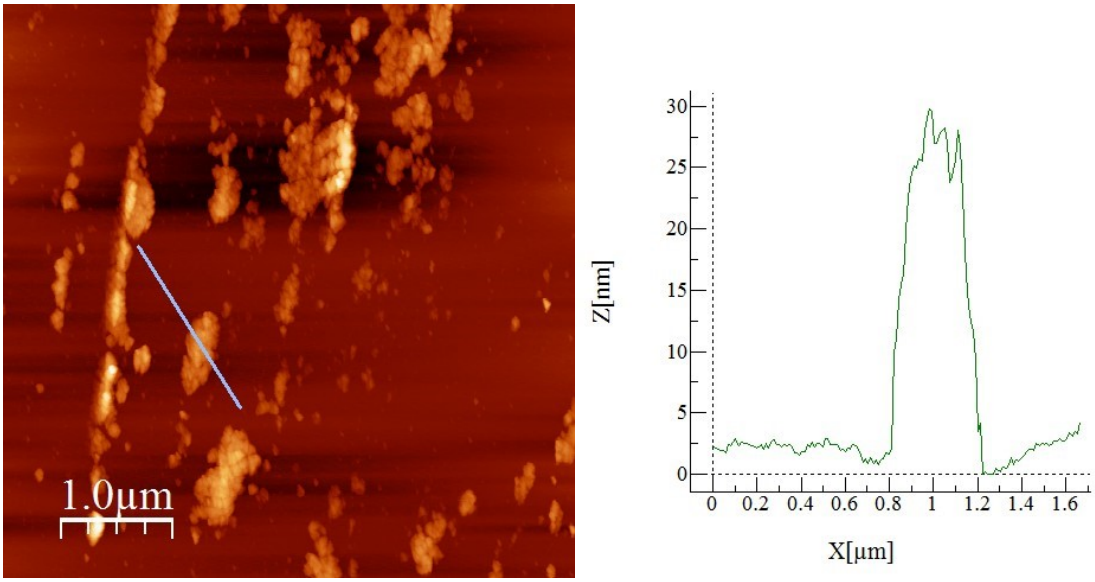

(a) (b)

Figure 17. (a) AFM image of H-NG with inset line indicating area of profile analysis. (b) Corresponding height profile analysis from AFM image.

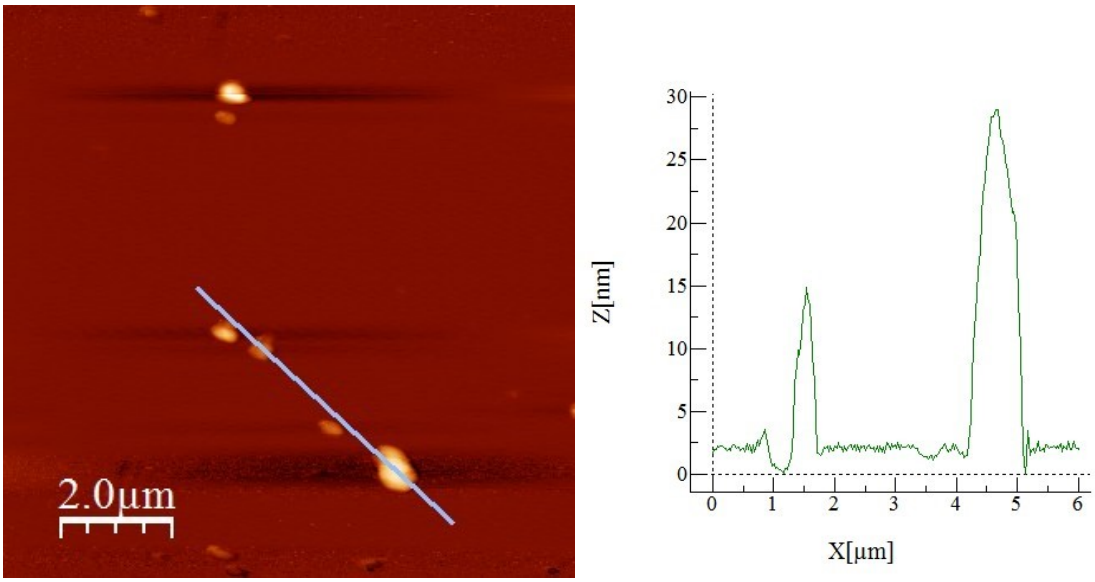

(a) (b)

Figure 18. (a) AFM image of F-NG with inset line indicating area of profile analysis. (b) Corresponding height profile analysis from AFM image.

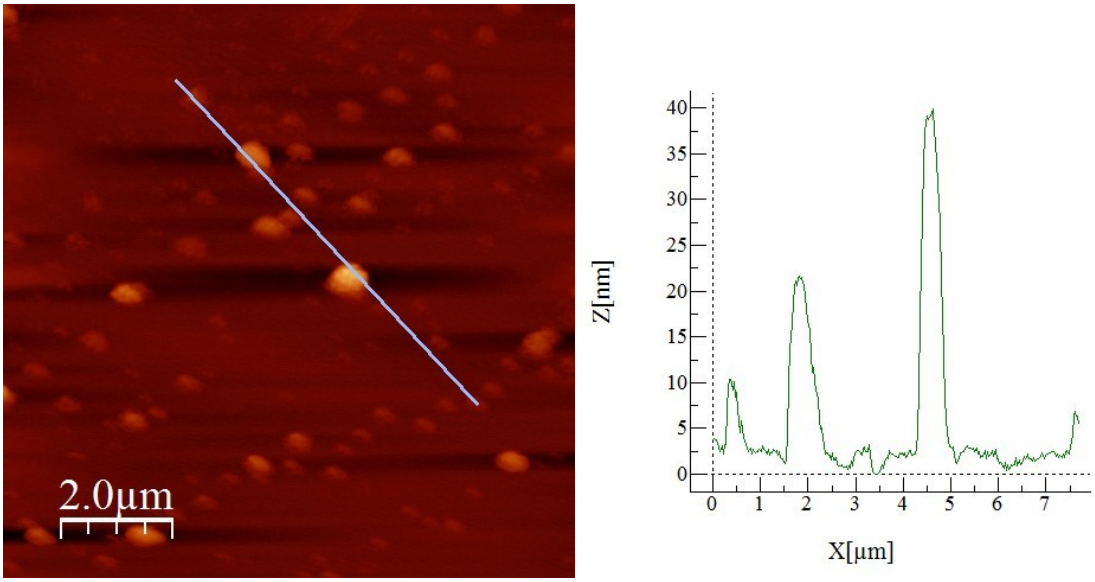

(a) (b)

Figure 19. (a) AFM images of HC-BCN Pune with inset line indicating area of profile of analysis. (b) Corresponding height profile from AFM image.

8.4 Electrochemistry of rGO, H-NG, F-NG, and HC-BCN Pune Modified Electrodes

CV's of a blank solution, containing only an acetonitrile solution of 0.1 M $TBAPF_6$, was collected after a nitrogen purge, (figure 20). The CV's indicate there still remains some active species in solution, presumably water, affecting the retrieval of totally blank CV's. However, the different materials do have a different response to the blank cell, notably the pseudocapacitive response of H-NG.

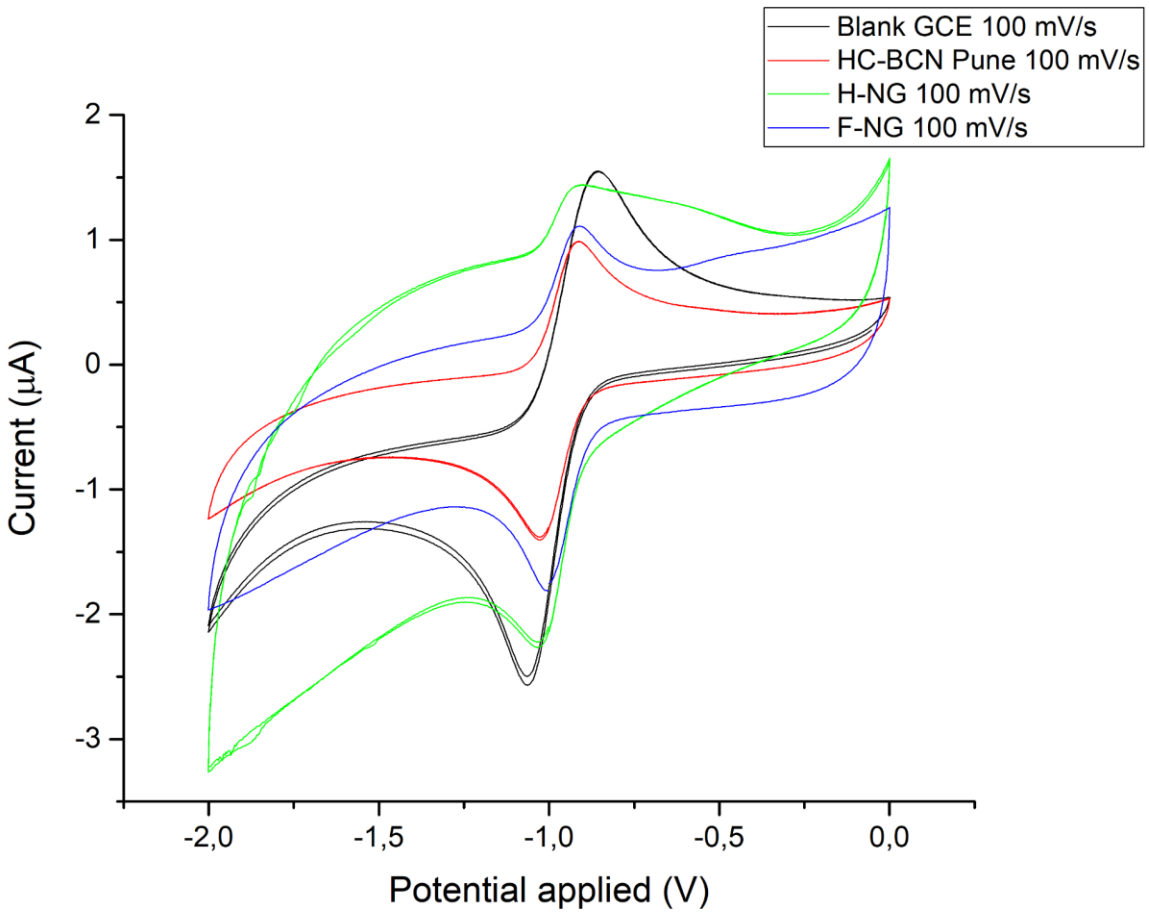

Figure 20. CV's blank GCE, HC-BCN Pune, H-NG, and F-NG in a solution of 0.1 M $TBAPF_6$ in acetonitrile.

Upon analyzing the CV's in 1 mM 4-NP in 0.1 M TBAPF6 acetonitrile solution the differences between the materials became quite stark. H-NG continues to show a pseudocapacitive-type CV with rGO and HC-BCN pune also showing CV's that lack some of the defined features of GCE and F-NG. rGO and H-NG seem to show a similar current response, especially at the negative end of the potential window and the reduction peak at approximately -1.00 V. All materials show a reduction peak at approximately -1.90 V and concomitant oxidation peak at approximately -1.80 V. The reduction peak observed at -1.00 V is complicated by the presence of the contaminant in solution observed in the blank cell. However, only the blank GCE shows a reversible peak at -1.00 V suggesting that at least in the case of GCE the contaminant observed in the blank cell response does affect the CV in the 4-NP reduction. There is the presence of an irreversible reduction peak

on the GCE and F-NG trace at -0.84 V and -0.76 V, respectively, which is conspicuously absent in the other materials.

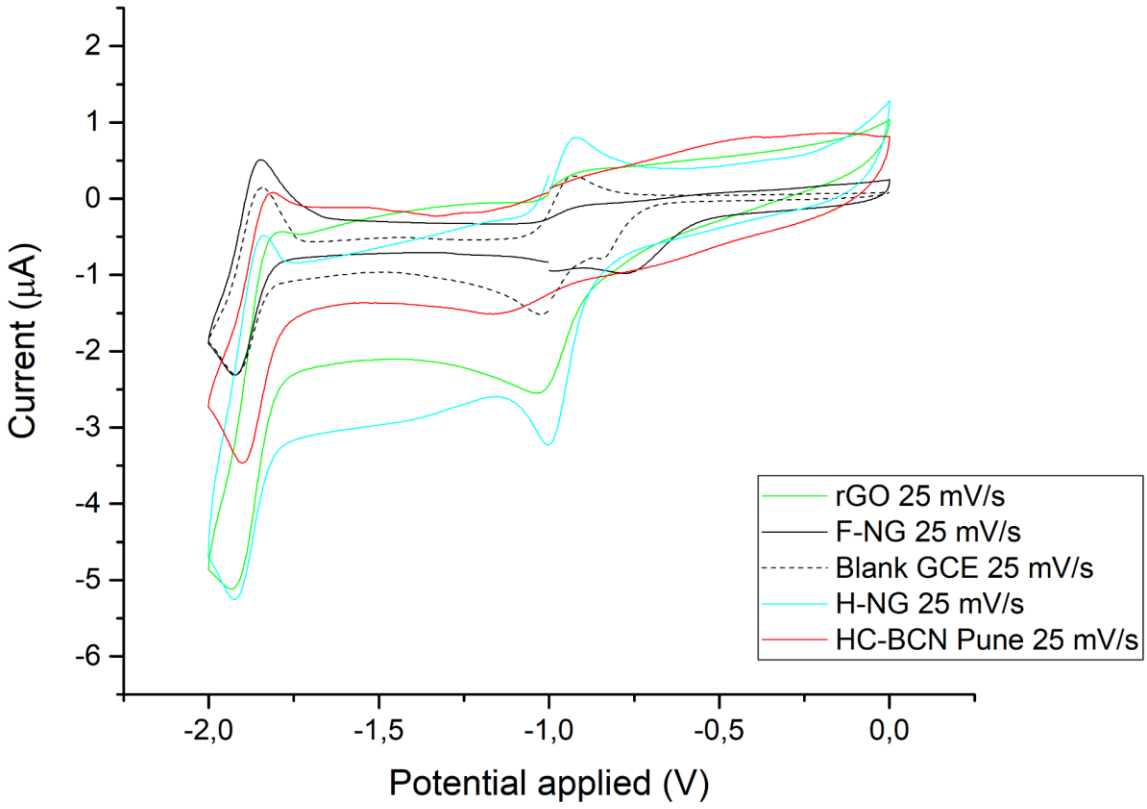

Figure 21. CV's of HC-BCN Pune, rGO, F-NG, Blank GCE, and H-NG collected at 25 mV/s with two traces each in a solution of 1 mM 4-NP in 0.1M $TBAPF_6$ in acetonitrile.

A reduced potential window was used to try and reacquire this peak in the remaining materials, see figure 22. In the CV's with reduced potential window the semblance of a reduction peak at approximately -0.75 V is observed and appears to show irreversible behavior.

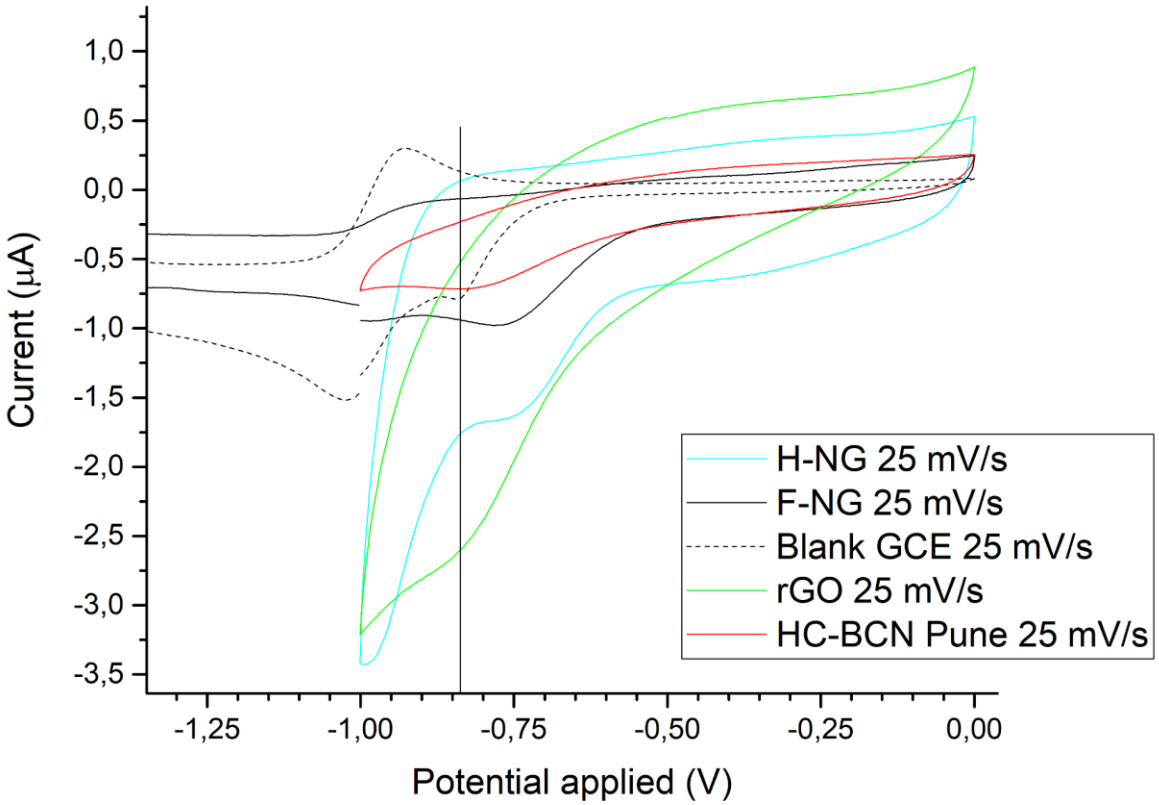

Figure 22. CV's of H-NG, F-NG, blank GCE, rGO, and HC-BCN Pune In a acetonitrile solution of 1mM 4-NP and 0.1M $TBAPF_6$, through line for comparison purposes.

F-NG and H-NG both show a reduction peak at -0.77 V whereas the blank GCE showed a reduction peak at -0.84 V. This observation suggests that there is an electrocatalytic effect for F-NG and H-NG in both increase in cathodic peak current and lower potential for the first reduction.

Richard Compton's group at Oxford University have explored the electrochemical reduction of 4-NP and offer a point of comparison for the CV's collected here.[94] From the Compton paper it can be surmised that the process which is being attenuated by the GRM's prepared in this work is associated with the initial reduction of 4-NP to the radical anion and the split-wave character is due to the increase in concentration within the reaction layer of an electroactive species which is then consumed resulting in the following larger wave.[94] So, it can be inferred from this that the

presence of nitrogen in the modified electrode aids in catalyzing the initial formation of the 4-NP radical anion.

While F-NG and H-NG have a very similar reduction potential at -0.77 V their current response shows a difference. From the different characterization methods used the materials are very different in structure, nitrogen content/functionality, as well as their oxygen content. F-NG contains graphitic nitrogen and some amount of nitrogen heterocycles while H-NG has nitrogen groups in edge or defect-type functional groups. Based on the current response of rGO it could be proffered that oxygen content present in a GRM is the likely source of this attenuated current response. The HC-BCN Pune modified electrode may offer a window on this as well, which is a material with a higher nitrogen content than either H-NG or F-NG in addition to having oxygen. Curiously HC-BCN Pune has quite weak current response by comparison, which may be due to the inclusion of boron, though it does show a slightly attenuated reduction potential compared to GCE.

9. Conclusion

Two nitrogen-doped GRM's were prepared utilizing different synthesis methods which were characterized by FTIR, XPS, Raman, SEM, and AFM. Characterization showed that the two materials, F-NG and H-NG, were similar but with key differences in their composition and structure. XPS unequivocally showed that the GRM's were both nitrogen-doped and that F-NG and H-NG had differing nitrogen functionality present. However, corroborating FTIR, Raman and XPS spectra of F-NG showed that it is most likely a material with multiple phases, in parts having the character of graphitic carbon nitride, many layer graphene, or amorphous carbon. The Raman analysis of structure of H-NG roughly followed the change of the material from stock GO, to rGO, and finally H-NG. The inclusion of a sample of GRM, HC-BCN Pune, prepared at university research partner CSIR-National Chemical Laboratory Pune India was included as comparison. Finally, the materials presented were coated onto glassy carbon electrodes and used for electrochemical reduction of 4-NP. F-NG, H-NG, and HC-BCN Pune were all capable of efficiently reducing 4-NP while showing unique electrochemical responses. H-NG and F-NG showed the ability to lower the reduction potential of the first electrochemical step, the reduction

of 4-NP to the radical anion. The key differences in the electrochemical response was conjectured to have been due to the presence of different nitrogen functionality. In closing, as the overview of chemistry, preparation methods, presented experimental results, and thinking in research demonstrate, the main issue with GRM's is preparing rationally designed GRM's with pinpoint atom-to-atom accuracy in synthesis that synthetic organic chemistry has achieved. By being able to impart specific defects, functional groups, and edge chirality at high precision and accuracy it would greatly enhance the ability to mobilize GRM's for specific applications. The bulwark of graphene basic research is close to being complete, as close to complete as any field of science can be, as such it points to the development of other 2D nanomaterials and engineers to apply them skillfully to problems that face society.

10. References

(1) MacNaught, A. D. *Compendium of Chemical Terminology*, 2. ed.; Blackwell Science: Oxford [u.a.], 1997. https://doi.org/10.1351/goldbook.G02683.

(2) Novoselov, K. S.; Geim, A. K.; Morozov, S. V.; Jiang, D.; Zhang, Y.; Dubonos, S. V.; Grigorieva, I. V.; Firsov, A. A. Electric Field Effect in Atomically Thin Carbon Films. *Science* **2004**, *306* (5696), 666–669. https://doi.org/10.1126/science.1102896.

(3) Geim, A. K. Graphene Prehistory. *Physica scripta* **2012**, *T146* (Journal Article), 14003. https://doi.org/10.1088/0031-8949/2012/T146/014003.

(4) Lerf, A.; He, H.; Forster, M.; Klinowski, J. Structure of Graphite Oxide Revisited. *J. Phys. Chem. B* **1998**, *102* (23), 4477–4482. https://doi.org/10.1021/jp9731821.

(5) KROTO, H. W.; HEATH, J. R.; O'BRIEN, S. C.; CURL, R. F.; SMALLEY, R. E. C60: Buckminsterfullerene. *Nature (London)* **1985**, *318* (6042), 162–163. https://doi.org/10.1038/318162a0.

(6) Oberlin, A.; Endo, M.; Koyama, T. Filamentous Growth of Carbon through Benzene Decomposition. *Journal of crystal growth* **1976**, *32* (3), 335–349. https://doi.org/10.1016/0022-0248(76)90115-9.

(7) Scopus. *Scopus Citation Search*. scopus.com (accessed 2021-08-12).

(8) Bianco, A.; Cheng, H.-M.; Enoki, T.; Gogotsi, Y.; Hurt, R. H.; Koratkar, N.; Kyotani, T.; Monthioux, M.; Park, C. R.; Tascon, J. M. D.; Zhang, J. All in the Graphene Family – A Recommended Nomenclature for Two-Dimensional Carbon Materials. *Carbon (New York)* **2013**, *65* (Journal Article), 1–6. https://doi.org/10.1016/j.carbon.2013.08.038.

(9) Wick, P.; Louw-Gaume, A. E.; Kucki, M.; Krug, H. F.; Kostarelos, K.; Fadeel, B.; Dawson, K. A.; Salvati, A.; Vázquez, E.; Ballerini, L.; Tretiach, M.; Benfenati, F.; Flahaut, E.; Gauthier, L.; Prato, M.; Bianco, A. Classification Framework for Graphene-Based Materials. *Angewandte Chemie (International ed.)* **2014**, *53* (30), 7714–7718. https://doi.org/10.1002/anie.201403335.

(10) Novoselov, K. S.; Geim, A. K.; Morozov, S. V.; Jiang, D.; Katsnelson, M. I.; Grigorieva, I. V.; Dubonos, S. V.; Firsov, A. A. Two-Dimensional Gas of Massless Dirac Fermions in Graphene. *Nature* **2005**, *438* (7065), 197–200. https://doi.org/10.1038/nature04233.

(11) Ritter, K. A.; Lyding, J. W. The Influence of Edge Structure on the Electronic Properties of Graphene Quantum Dots and Nanoribbons. *Nature materials* **2009**, *8* (3), 235–242.

https://doi.org/10.1038/nmat2378.

(12) Acik, M.; Chabal, Y. J. Nature of Graphene Edges: A Review. *Jpn J Appl Phys* **2011**, *50* (7), 070101–070116. https://doi.org/10.1143/JJAP.50.070101.

(13) Koskinen, P.; Malola, S.; Häkkinen, H. Evidence for Graphene Edges beyond Zigzag and Armchair. *Physical review. B, Condensed matter and materials physics* **2009**, *80* (7). https://doi.org/10.1103/PhysRevB.80.073401.

(14) Pérez, E. M.; Martín, N. π-π Interactions in Carbon Nanostructures. *Chemical Society reviews* **2015**, *44* (18), 6425–6433. https://doi.org/10.1039/c5cs00578g.

(15) Ma, J.; Alfè, D.; Michaelides, A.; Wang, E. Stone-Wales Defects in Graphene and Other Planar s p 2 -Bonded Materials. *Phys. Rev. B* **2009**, *80* (3), 033407. https://doi.org/10.1103/PhysRevB.80.033407.

(16) Bissett, M. A.; Konabe, S.; Okada, S.; Tsuji, M.; Ago, H. Enhanced Chemical Reactivity of Graphene Induced by Mechanical Strain. *ACS nano* **2013**, *7* (11), 10335–10343. https://doi.org/10.1021/nn404746h.

(17) Niyogi, S.; Bekyarova, E.; Itkis, M. E.; McWilliams, J. L.; Hamon, M. A.; Haddon, R. C. Solution Properties of Graphite and Graphene. *J. Am. Chem. Soc.* **2006**, *128* (24), 7720–7721. https://doi.org/10.1021/ja060680r.

(18) Georgakilas, V.; Otyepka, M.; Bourlinos, A. B.; Chandra, V.; Kim, N.; Kemp, K. C.; Hobza, P.; Zboril, R.; Kim, K. S. Functionalization of Graphene: Covalent and Non-Covalent Approaches, Derivatives and Applications. *Chem. Rev.* **2012**, *112* (11), 6156–6214. https://doi.org/10.1021/cr3000412.

(19) Dreyer, D. R.; Park, S.; Bielawski, C. W.; Ruoff, R. S. The Chemistry of Graphene Oxide. *Chemical Society Reviews* **2009**, *39* (1), 228–24. https://doi.org/10.1039/b917103g.

(20) Paredes, J. I.; Villar-Rodil, S.; Martínez-Alonso, A.; Tascón, J. M. D. Graphene Oxide Dispersions in Organic Solvents. *Langmuir* **2008**, *24* (19), 10560–10564. https://doi.org/10.1021/la801744a.

(21) Sarkar, S.; Bekyarova, E.; Haddon, R. C. Chemistry at the Dirac Point: Diels–Alder Reactivity of Graphene. *Accounts of chemical research* **2012**, *45* (4), 673–682. https://doi.org/10.1021/ar200302g.

(22) Daukiya, L.; Mattioli, C.; Aubel, D.; Hajjar-Garreau, S.; Vonau, F.; Denys, E.; Reiter, G.; Fransson, J.; Perrin, E.; Bocquet, M.-L.; Bena, C.; Gourdon, A.; Simon, L. Covalent

Functionalization by Cycloaddition Reactions of Pristine Defect-Free Graphene. *ACS Nano* **2017**, *11* (1), 627–634. https://doi.org/10.1021/acsnano.6b06913.

(23) Quintana, M.; Spyrou, K.; Grzelczak, M.; Browne, W. R.; Rudolf, P.; Prato, M. Functionalization of Graphene via 1,3-Dipolar Cycloaddition. *ACS Nano* **2010**, *4* (6), 3527–3533. https://doi.org/10.1021/nn100883p.

(24) Yang, X.; Chen, F.; Kim, M. A.; Liu, H.; Wolf, L. M.; Yan, M. On the Reactivity Enhancement of Graphene by Metallic Substrates towards Aryl Nitrene Cycloadditions. *Chemistry – A European Journal* **2021**, *27* (29), 7887–7896. https://doi.org/10.1002/chem.202100227.

(25) Bekyarova, E.; Itkis, M. E.; Ramesh, P.; Berger, C.; Sprinkle, M.; de Heer, W. A.; Haddon, R. C. Chemical Modification of Epitaxial Graphene: Spontaneous Grafting of Aryl Groups. *J. Am. Chem. Soc.* **2009**, *131* (4), 1336–1337. https://doi.org/10.1021/ja8057327.

(26) Bahr, J. L.; Yang, J.; Kosynkin, D. V.; Bronikowski, M. J.; Smalley, R. E.; Tour, J. M. Functionalization of Carbon Nanotubes by Electrochemical Reduction of Aryl Diazonium Salts: A Bucky Paper Electrode. *J. Am. Chem. Soc.* **2001**, *123* (27), 6536–6542. https://doi.org/10.1021/ja010462s.

(27) Liu, Y.-C.; McCreery, R. L. Reactions of Organic Monolayers on Carbon Surfaces Observed with Unenhanced Raman Spectroscopy. *J. Am. Chem. Soc.* **1995**, *117* (45), 11254–11259. https://doi.org/10.1021/ja00150a024.

(28) Delamar, M.; Hitmi, R.; Pinson, J.; Saveant, J. M. Covalent Modification of Carbon Surfaces by Grafting of Functionalized Aryl Radicals Produced from Electrochemical Reduction of Diazonium Salts. *J. Am. Chem. Soc.* **1992**, *114* (14), 5883–5884. https://doi.org/10.1021/ja00040a074.

(29) Dimiev, A. M.; Tour, J. M. Mechanism of Graphene Oxide Formation. *ACS Nano* **2014**, *8* (3), 3060–3068. https://doi.org/10.1021/nn500606a.

(30) Hummers, W. S.; Offeman, R. E. Preparation of Graphitic Oxide. *Journal of the American Chemical Society* **1958**, *80* (6), 1339. https://doi.org/10.1021/ja01539a017.

(31) Marcano, D. C.; Kosynkin, D. V.; Berlin, J. M.; Sinitskii, A.; Sun, Z.; Slesarev, A.; Alemany, L. B.; Lu, W.; Tour, J. M. Improved Synthesis of Graphene Oxide. *ACS nano* **2010**, *4* (8), 4806–4814. https://doi.org/10.1021/nn1006368.

(32) HIRATA, M.; GOTOU, T.; HORIUCHI, S.; FUJIWARA, M.; OHBA, M. Thin-Film

Particles of Graphite Oxide 1:High-Yield Synthesis and Flexibility of the Particles. *Carbon (New York)* **2004**, *42* (14), 2929–2937. https://doi.org/10.1016/S0008-6223(04)00444-0.

(33) Stankovich, S.; Dikin, D. A.; Piner, R. D.; Kohlhaas, K. A.; Kleinhammes, A.; Jia, Y.; Wu, Y.; Nguyen, S. T.; Ruoff, R. S. Synthesis of Graphene-Based Nanosheets via Chemical Reduction of Exfoliated Graphite Oxide. *Carbon (New York)* **2007**, *45* (7), 1558–1565. https://doi.org/10.1016/j.carbon.2007.02.034.

(34) Shin, H.; Kim, K. K.; Benayad, A.; Yoon, S.; Park, H. K.; Jung, I.; Jin, M. H.; Jeong, H.; Kim, J. M.; Choi, J.; Lee, Y. H. Efficient Reduction of Graphite Oxide by Sodium Borohydride and Its Effect on Electrical Conductance. *Advanced functional materials* **2009**, *19* (12), 1987–1992. https://doi.org/10.1002/adfm.200900167.

(35) Zhang, J.; Yang, H.; Shen, G.; Cheng, P.; Zhang, J.; Guo, S. Reduction of Graphene Oxide ViaL-Ascorbic Acid. *Chem. Commun.* **2010**, *46* (7), 1112–1114. https://doi.org/10.1039/B917705A.

(36) Fernández-Merino, M. J.; Guardia, L.; Paredes, J. I.; Villar-Rodil, S.; Solís-Fernández, P.; Martínez-Alonso, A.; Tascón, J. M. D. Vitamin C Is an Ideal Substitute for Hydrazine in the Reduction of Graphene Oxide Suspensions. *J. Phys. Chem. C* **2010**, *114* (14), 6426–6432. https://doi.org/10.1021/jp100603h.

(37) Bo, Z.; Shuai, X.; Mao, S.; Yang, H.; Qian, J.; Chen, J.; Yan, J.; Cen, K. Green Preparation of Reduced Graphene Oxide for Sensing and Energy Storage Applications. *Sci Rep* **2014**, *4* (1), 4684. https://doi.org/10.1038/srep04684.

(38) Zhou, Y.; Bao, Q.; Tang, L. A. L.; Zhong, Y.; Loh, K. P. Hydrothermal Dehydration for the "Green" Reduction of Exfoliated Graphene Oxide to Graphene and Demonstration of Tunable Optical Limiting Properties. *Chemistry of materials* **2009**, *21* (13), 2950–2956. https://doi.org/10.1021/cm9006603.

(39) Rabenau, A. The Role of Hydrothermal Synthesis in Preparative Chemistry. *Angewandte Chemie International Edition in English* **1985**, *24* (12), 1026–1040. https://doi.org/10.1002/anie.198510261.

(40) Sasikala, S. P.; Poulin, P.; Aymonier, C. Advances in Subcritical Hydro-/Solvothermal Processing of Graphene Materials. *Advanced Materials* **2017**, *29* (22), 1605473. https://doi.org/10.1002/adma.201605473.

(41) Savage, P. E. Organic Chemical Reactions in Supercritical Water. *Chem. Rev.* **1999**, *99* (2),

603–622. https://doi.org/10.1021/cr9700989.

(42) Sawyer, D. T.; Roberts, J. L. Hydroxide Ion: An Effective One-Electron Reducing Agent? *Acc. Chem. Res.* **1988**, *21* (12), 469–476. https://doi.org/10.1021/ar00156a006.

(43) Seo, M.; Yoon, D.; Hwang, K. S.; Kang, J. W.; Kim, J. Supercritical Alcohols as Solvents and Reducing Agents for the Synthesis of Reduced Graphene Oxide. *Carbon* **2013**, *64*, 207–218. https://doi.org/10.1016/j.carbon.2013.07.053.

(44) Huang, H.-H.; De Silva, K. K. H.; Kumara, G. R. A.; Yoshimura, M. Structural Evolution of Hydrothermally Derived Reduced Graphene Oxide. *Sci Rep* **2018**, *8* (1), 6849. https://doi.org/10.1038/s41598-018-25194-1.

(45) Acik, M.; Lee, G.; Mattevi, C.; Pirkle, A.; Wallace, R. M.; Chhowalla, M.; Cho, K.; Chabal, Y. The Role of Oxygen during Thermal Reduction of Graphene Oxide Studied by Infrared Absorption Spectroscopy. *J. Phys. Chem. C* **2011**, *115* (40), 19761–19781. https://doi.org/10.1021/jp2052618.

(46) Botas, C.; Álvarez, P.; Blanco, C.; Santamaría, R.; Granda, M.; Gutiérrez, M. D.; Rodríguez-Reinoso, F.; Menéndez, R. Critical Temperatures in the Synthesis of Graphene-like Materials by Thermal Exfoliation–Reduction of Graphite Oxide. *Carbon* **2013**, *52*, 476–485. https://doi.org/10.1016/j.carbon.2012.09.059.

(47) Eigler, S.; Grimm, S.; Enzelberger-Heim, M.; Müller, P.; Hirsch, A. Graphene Oxide: Efficiency of Reducing Agents. *Chemical Communications* **2013**, *49* (67), 7391–7393. https://doi.org/10.1039/C3CC43612H.

(48) McAllister, M. J.; Li, J.-L.; Adamson, D. H.; Schniepp, H. C.; Abdala, A. A.; Liu, J.; Herrera-Alonso, M.; Milius, D. L.; Car, R.; Prud'homme, R. K.; Aksay, I. A. Single Sheet Functionalized Graphene by Oxidation and Thermal Expansion of Graphite. *Chem. Mater.* **2007**, *19* (18), 4396–4404. https://doi.org/10.1021/cm0630800.

(49) Muñoz, R.; Gómez-Aleixandre, C. Review of CVD Synthesis of Graphene. *Chemical Vapor Deposition* **2013**, *19* (10-11–12), 297–322. https://doi.org/10.1002/cvde.201300051.

(50) Tavakoli, M. M.; Azzellino, G.; Hempel, M.; Lu, A.-Y.; Martin-Martinez, F. J.; Zhao, J.; Yeo, J.; Palacios, T.; Buehler, M. J.; Kong, J. Synergistic Roll-to-Roll Transfer and Doping of CVD-Graphene Using Parylene for Ambient-Stable and Ultra-Lightweight Photovoltaics. *Advanced Functional Materials* **2020**, *30* (31), 2001924. https://doi.org/10.1002/adfm.202001924.

(51) Sun, J.; Chen, Y.; Priydarshi, M. Kr.; Chen, Z.; Bachmatiuk, A.; Zou, Z.; Chen, Z.; Song, X.; Gao, Y.; Rümmeli, M. H.; Zhang, Y.; Liu, Z. Direct Chemical Vapor Deposition-Derived Graphene Glasses Targeting Wide Ranged Applications. *Nano Lett.* **2015**, *15* (9), 5846–5854. https://doi.org/10.1021/acs.nanolett.5b01936.

(52) Narita, A.; Wang, X.-Y.; Feng, X.; Müllen, K. New Advances in Nanographene Chemistry. *Chemical Society Reviews* **2015**, *44* (18), 6616–6643. https://doi.org/10.1039/C5CS00183H.

(53) Wu, J.; Pisula, W.; Müllen, K. Graphenes as Potential Material for Electronics. *Chem. Rev.* **2007**, *107* (3), 718–747. https://doi.org/10.1021/cr068010r.

(54) Simpson, C. D.; Brand, J. D.; Berresheim, A. J.; Przybilla, L.; Räder, H. J.; Müllen, K. Synthesis of a Giant 222 Carbon Graphite Sheet. *Chemistry – A European Journal* **2002**, *8* (6), 1424–1429. https://doi.org/10.1002/1521-3765(20020315)8:6<1424::AID-CHEM1424>3.0.CO;2-Z.

(55) Cai, J.; Ruffieux, P.; Jaafar, R.; Bieri, M.; Braun, T.; Blankenburg, S.; Muoth, M.; Seitsonen, A. P.; Saleh, M.; Feng, X.; Müllen, K.; Fasel, R. Atomically Precise Bottom-up Fabrication of Graphene Nanoribbons. *Nature* **2010**, *466* (7305), 470–473. https://doi.org/10.1038/nature09211.

(56) Lv, R.; Terrones, M. Towards New Graphene Materials: Doped Graphene Sheets and Nanoribbons. *Materials Letters* **2012**, *78*, 209–218. https://doi.org/10.1016/j.matlet.2012.04.033.

(57) Artyushkova, K. Misconceptions in Interpretation of Nitrogen Chemistry from X-Ray Photoelectron Spectra. *Journal of vacuum science & technology. A, Vacuum, surfaces, and films* **2020**, *38* (3), 31002. https://doi.org/10.1116/1.5135923.

(58) Li, X.; Wang, H.; Robinson, J. T.; Sanchez, H.; Diankov, G.; Dai, H. Simultaneous Nitrogen Doping and Reduction of Graphene Oxide. *J. Am. Chem. Soc.* **2009**, *131* (43), 15939–15944. https://doi.org/10.1021/ja907098f.

(59) Long, D.; Li, W.; Ling, L.; Miyawaki, J.; Mochida, I.; Yoon, S.-H. Preparation of Nitrogen-Doped Graphene Sheets by a Combined Chemical and Hydrothermal Reduction of Graphene Oxide. *Langmuir* **2010**, *26* (20), 16096–16102. https://doi.org/10.1021/la102425a.

(60) Deng, D.; Pan, X.; Yu, L.; Cui, Y.; Jiang, Y.; Qi, J.; Li, W.-X.; Fu, Q.; Ma, X.; Xue, Q.;

Sun, G.; Bao, X. Toward N-Doped Graphene via Solvothermal Synthesis. *Chem. Mater.* **2011**, *23* (5), 1188–1193. https://doi.org/10.1021/cm102666r.

(61) Wei, D.; Liu, Y.; Wang, Y.; Zhang, H.; Huang, L.; Yu, G. Synthesis of N-Doped Graphene by Chemical Vapor Deposition and Its Electrical Properties. *Nano Lett.* **2009**, *9* (5), 1752–1758. https://doi.org/10.1021/nl803279t.

(62) Qu, L.; Liu, Y.; Baek, J.-B.; Dai, L. Nitrogen-Doped Graphene as Efficient Metal-Free Electrocatalyst for Oxygen Reduction in Fuel Cells. *ACS Nano* **2010**, *4* (3), 1321–1326. https://doi.org/10.1021/nn901850u.

(63) Li, X.-H.; Kurasch, S.; Kaiser, U.; Antonietti, M. Synthesis of Monolayer-Patched Graphene from Glucose. *Angewandte Chemie International Edition* **2012**, *51* (38), 9689–9692. https://doi.org/10.1002/anie.201203207.

(64) Yang, H. B.; Miao, J.; Hung, S.-F.; Chen, J.; Tao, H. B.; Wang, X.; Zhang, L.; Chen, R.; Gao, J.; Chen, H. M.; Dai, L.; Liu, B. Identification of Catalytic Sites for Oxygen Reduction and Oxygen Evolution in N-Doped Graphene Materials: Development of Highly Efficient Metal-Free Bifunctional Electrocatalyst. *Science Advances* **2016**. https://doi.org/10.1126/sciadv.1501122.

(65) Ferrari, A. C.; Basko, D. M. Raman Spectroscopy as a Versatile Tool for Studying the Properties of Graphene. *Nature nanotechnology* **2013**, *8* (4), 235–246. https://doi.org/10.1038/nnano.2013.46.

(66) Malard, L. M.; Pimenta, M. A.; Dresselhaus, G.; Dresselhaus, M. S. Raman Spectroscopy in Graphene. *Physics reports* **2009**, *473* (5), 51–87. https://doi.org/10.1016/j.physrep.2009.02.003.

(67) Eigler, S.; Hof, F.; Enzelberger-Heim, M.; Grimm, S.; Müller, P.; Hirsch, A. Statistical Raman Microscopy and Atomic Force Microscopy on Heterogeneous Graphene Obtained after Reduction of Graphene Oxide. *Journal of physical chemistry. C* **2014**, *118* (14), 7698–7704. https://doi.org/10.1021/jp500580g.

(68) Rance, G. A.; Marsh, D. H.; Nicholas, R. J.; Khlobystov, A. N. UV–Vis Absorption Spectroscopy of Carbon Nanotubes: Relationship between the π-Electron Plasmon and Nanotube Diameter. *Chemical physics letters* **2010**, *493* (1), 19–23. https://doi.org/10.1016/j.cplett.2010.05.012.

(69) Baer, D. R.; Artyushkova, K.; Richard Brundle, C.; Castle, J. E.; Engelhard, M. H.; Gaskell,

K. J.; Grant, J. T.; Haasch, R. T.; Linford, M. R.; Powell, C. J.; Shard, A. G.; Sherwood, P. M. A.; Smentkowski, V. S. Practical Guides for X-Ray Photoelectron Spectroscopy: First Steps in Planning, Conducting, and Reporting XPS Measurements. *Journal of vacuum science & technology. A, Vacuum, surfaces, and films* **2019**, *37* (3), 31401. https://doi.org/10.1116/1.5065501.

(70) Meyer, J. C. 5 - Transmission Electron Microscopy (TEM) of Graphene. In *Graphene*; Elsevier Ltd, 2014; pp 101–123. https://doi.org/10.1533/9780857099334.2.101.

(71) Shearer, C. J.; Slattery, A. D.; Stapleton, A. J.; Shapter, J. G.; Gibson, C. T. Accurate Thickness Measurement of Graphene. *NANO* **2016**, *27* (12), 125704. https://doi.org/10.1088/0957-4484/27/12/125704.

(72) Daelemans, B.; Bilbao, N.; Dehaen, W.; De Feyter, S. Carbocatalysis with Pristine Graphite: On-Surface Nanochemistry Assists Solution-Based Catalysis. *Chemical Society reviews* **2021**, *50* (4), 2280–2296. https://doi.org/10.1039/D0CS01294G.

(73) Rasool, H. I.; Song, E. B.; Mecklenburg, M.; Regan, B. C.; Wang, K. L.; Weiller, B. H.; Gimzewski, J. K. Atomic-Scale Characterization of Graphene Grown on Copper (100) Single Crystals. *Journal of the American Chemical Society* **2011**, *133* (32), 12536–12543. https://doi.org/10.1021/ja200245p.

(74) Decker, R.; Wang, Y.; Brar, V. W.; Regan, W.; Tsai, H.-Z.; Wu, Q.; Gannett, W.; Zettl, A.; Crommie, M. F. Local Electronic Properties of Graphene on a BN Substrate via Scanning Tunneling Microscopy. *Nano letters* **2011**, *11* (6), 2291–2295. https://doi.org/10.1021/nl2005115.

(75) Ye, R.; Dong, J.; Wang, L.; Mendoza-Cruz, R.; Li, Y.; An, P.-F.; Yacamán, M. J.; Yakobson, B. I.; Chen, D.; Tour, J. M. Manganese Deception on Graphene and Implications in Catalysis. *Carbon* **2018**, *132* (Generic), 623–631. https://doi.org/10.1016/j.carbon.2018.02.082.

(76) Weatherup, R. S.; Bayer, B. C.; Blume, R.; Ducati, C.; Baehtz, C.; Schlögl, R.; Hofmann, S. In Situ Characterization of Alloy Catalysts for Low-Temperature Graphene Growth. *Nano letters* **2011**, *11* (10), 4154–4160. https://doi.org/10.1021/nl202036y.

(77) Viinikanoja, A.; Kauppila, J.; Damlin, P.; Suominen, M.; Kvarnström, C. In Situ FTIR and Raman Spectroelectrochemical Characterization of Graphene Oxide upon Electrochemical Reduction in Organic Solvents. *Phys. Chem. Chem. Phys.* **2015**, *17* (18), 12115–12123.

https://doi.org/10.1039/C5CP00942A.

(78) Giribabu, K.; Suresh, R.; Manigandan, R.; Praveen Kumar, S.; Muthamizh, S.; Munusamy, S.; Narayanan, V. Preparation of Nitrogen-Doped Reduced Graphene Oxide and Its Use in a Glassy Carbon Electrode for Sensing 4-Nitrophenol at Nanomolar Levels. *Microchim Acta* **2014**, *181* (15–16), 1863–1870. https://doi.org/10.1007/s00604-014-1251-4.

(79) Zhang, Y.; Wu, L.; Lei, W.; Xia, X.; Xia, M.; Hao, Q. Electrochemical Determination of 4-Nitrophenol at Polycarbazole/N-Doped Graphene Modified Glassy Carbon Electrode. *Electrochimica acta* **2014**, *146* (Journal Article), 568–576. https://doi.org/10.1016/j.electacta.2014.08.153.

(80) Kong, X.; Sun, Z.; Chen, M.; Chen, C.; Chen, Q. Metal-Free Catalytic Reduction of 4-Nitrophenol to 4-Aminophenol by N-Doped Graphene. *Energy Environ. Sci.* **2013**, *6* (11), 3260. https://doi.org/10.1039/c3ee40918j.

(81) Zhang, Y.; Fugane, K.; Mori, T.; Niu, L.; Ye, J. Wet Chemical Synthesis of Nitrogen-Doped Graphene towards Oxygen Reduction Electrocatalysts without High-Temperature Pyrolysis. *Journal of Materials Chemistry* **2012**, *22* (14), 6575–6580.

(82) Liu, S.; Yang, H.; Huang, X.; Liu, L.; Cai, W.; Gao, J.; Li, X.; Zhang, T.; Huang, Y.; Liu, B. Identifying Active Sites of Nitrogen-Doped Carbon Materials for the CO2 Reduction Reaction. *Adv.Funct.Mater.* **2018**, *28* (21), 1800499. https://doi.org/10.1002/adfm.201800499.

(83) Socrates, G. *Infrared and Raman Characteristic Group Frequencies: Tables and Charts*, 3. ed., repr. as paperback.; Wiley: Chichester, 2010.

(84) Ossonon, B. D.; Bélanger, D. Synthesis and Characterization of Sulfophenyl-Functionalized Reduced Graphene Oxide Sheets. *RSC Adv.* **2017**, *7* (44), 27224–27234. https://doi.org/10.1039/C6RA28311J.

(85) Ahn, S. I.; Kim, K.; Kim, J. Y.; Kim, E. S.; Han, J. Y.; Eom, J. W.; Choi, K.-K.; Park, J.-C.; Kim, S.-H.; Jeong, E. D.; Choi, K. C. Reduction Intermediates of Graphene Oxide for Low Temperature Reduction Electrode Material. *RSC Adv.* **2014**, *4* (43), 22476–22480. https://doi.org/10.1039/C4RA01472C.

(86) Shcherban, N. D.; Mäki-Arvela, P.; Aho, A.; Sergiienko, S. A.; Yaremov, P. S.; Eränen, K.; Murzin, D. Y. Melamine-Derived Graphitic Carbon Nitride as a New Effective Metal-Free Catalyst for Knoevenagel Condensation of Benzaldehyde with Ethylcyanoacetate. *Catalysis*

science & technology **2018**, *8* (11), 2928–2937. https://doi.org/10.1039/C8CY00253C.

(87) Lotsch, B. V.; Schnick, W. New Light on an Old Story: Formation of Melam during Thermal Condensation of Melamine. *Chem. Eur. J.* **2007**, *13* (17), 4956–4968. https://doi.org/10.1002/chem.200601291.

(88) Li, X.; Zhang, J.; Shen, L.; Ma, Y.; Lei, W.; Cui, Q.; Zou, G. Preparation and Characterization of Graphitic Carbon Nitride through Pyrolysis of Melamine. *Appl. Phys. A* **2009**, *94* (2), 387–392. https://doi.org/10.1007/s00339-008-4816-4.

(89) Yamada, Y.; Tanaka, H.; Kubo, S.; Sato, S. Unveiling Bonding States and Roles of Edges in Nitrogen-Doped Graphene Nanoribbon by X-Ray Photoelectron Spectroscopy. *Carbon* **2021**, *185*, 342–367. https://doi.org/10.1016/j.carbon.2021.08.085.

(90) Zafar, Z.; Ni, Z. H.; Wu, X.; Shi, Z. X.; Nan, H. Y.; Bai, J.; Sun, L. T. Evolution of Raman Spectra in Nitrogen Doped Graphene. *Carbon* **2013**, *61* (Journal Article), 57–62.

(91) Schuepfer, D. B.; Badaczewski, F.; Guerra-Castro, J. M.; Hofmann, D. M.; Heiliger, C.; Smarsly, B.; Klar, P. J. Assessing the Structural Properties of Graphitic and Non-Graphitic Carbons by Raman Spectroscopy. *Carbon (New York)* **2020**, *161* (Journal Article), 359–372. https://doi.org/10.1016/j.carbon.2019.12.094.

(92) Jaafar, M. M.; Ciniciato, G. P. M. K.; Ibrahim, S. A.; Phang, S. M.; Yunus, K.; Fisher, A. C.; Iwamoto, M.; Vengadesh, P. Preparation of a Three-Dimensional Reduced Graphene Oxide Film by Using the Langmuir–Blodgett Method. *Langmuir* **2015**, *31* (38), 10426–10434. https://doi.org/10.1021/acs.langmuir.5b02708.

(93) Lerf, A.; He, H.; Riedl, T.; Forster, M.; Klinowski, J. 13C and 1H MAS NMR Studies of Graphite Oxide and Its Chemically Modified Derivatives. *Solid state ionics* **1997**, *101* (Journal Article), 857–862. https://doi.org/10.1016/S0167-2738(97)00319-6.

(94) Silvester, D. S.; Wain, A. J.; Aldous, L.; Hardacre, C.; Compton, R. G. Electrochemical Reduction of Nitrobenzene and 4-Nitrophenol in the Room Temperature Ionic Liquid [C 4dmim][N(Tf) 2]. *Journal of electroanalytical chemistry (Lausanne, Switzerland)* **2006**, *596* (2), 131–140. https://doi.org/10.1016/j.jelechem.2006.07.028.